Reliability-based settlement analysis of embankments over soft soils reinforced with T-shaped deep cement mixing piles

Chana Phutthananon, Pornkasem Jongpradist, Daniel Dias, Xiangfeng Guo, Pitthaya Jamsawang, Julien Baroth

Reliability-based settlement analysis of embankments over soft soils reinforced with T-shaped deep cement mixing piles

Journal:	*Frontiers of Structural and Civil Engineering*
Manuscript ID	FSCE-2021-0697
Manuscript Type:	Research Article
Date Submitted by the Author:	16-Nov-2021
Complete List of Authors:	Phutthananon, Chana; King Mongkut's University of Technology Thonburi, Department of Civil Engineering, Faculty of Engineering Jongpradist, Pornkasem ; King Mongkut's University of Technology Thonburi, Department of Civil Engineering, Faculty of Engineering Dias, Daniel; University Grenoble Alpes Guo, Xiangfeng; University Grenoble Alpes Jamsawang, Pitthaya; King Mongkut's University of Technology North Bangkok, Department of Civil Engineering Baroth, Julien; University Grenoble Alpes
Keywords:	T-shaped deep cement mixing piles, Piled embankments, Settlement, Reliability analysis, Soil uncertainties
Speciality:	Foundations < Geotechnical and Underground Engineering, Computer Modeling < Geotechnical and Underground Engineering

Reliability-based settlement analysis of embankments over soft soils reinforced with T-shaped deep cement mixing piles

Chana Phutthananon[a]

Postdoctoral Fellow

Pornkasem Jongpradist[a,*]

Associate Professor

Daniel Dias[b,c]

Professor

Xiangfeng Guo[b]

Postdoctoral Fellow

Pitthaya Jamsawang[d]

Professor

Julien Baroth[b]

Associate Professor

[a] Construction Innovations and Future Infrastructures Research Center, Department of Civil Engineering, Faculty of Engineering, King Mongkut's University of Technology Thonburi, Bangkok 10140, Thailand

[b] Univ. Grenoble Alpes, CNRS, Grenoble INP, 3SR, Grenoble 38000, France

[c] Antea Group, Antony 92160, France

[d] Soil Engineering Research Center, Department of Civil Engineering, King Mongkut's University of Technology North Bangkok, Bangkok 10800, Thailand

Submitted to: **Frontiers of Structural and Civil Engineering – Springer**

*Corresponding author: **Dr. Pornkasem Jongpradist**, Associate Professor
Department of Civil Engineering, Faculty of Engineering, King Mongkut's University of Technology Thonburi, 126 Pracha Uthit Rd., Bang Mod, Thung Khru, Bangkok 10140, Thailand, Phone: 662-470-9305, Fax: 662-427-9063, E-mail: pornkasem.jon@kmutt.ac.th

Number of words in main text: 7,983 (excluded from Abstract, Acknowledgments, and References)

Number of tables: 6

Number of figures: 13

Abstract

A reliability-based settlement analysis of T-shaped deep cement mixing (TDM) pile-supported embankments over soft soils is presented in this paper. The uncertainties of the mechanical properties of the in-situ soil, pile, and embankment and the effect of the pile shape are considered simultaneously. The analyses are performed using Monte Carlo simulations in combination with an adaptive Kriging. Individual and system failure probabilities in terms of the differential and maximum settlements (serviceability limit state (SLS) requirements) are considered. The reliability results for the embankments supported by TDM piles with various shapes are compared and discussed together with the results for conventional deep cement mixing piled embankments with equivalent pile volumes. The influences of the inherent variabilities in the material properties (mean and coefficient of variation values) on the reliability of the piled embankments are also investigated. This study shows that large TDM piles, particularly those with a shape factor of greater than 3, can enhance the reliability of the embankment in terms of SLS requirements and even avoid unacceptable reliability levels caused by variability in the material properties.

Keywords: T-shaped deep cement mixing piles; Piled embankments; Settlement; Reliability analysis; Soil uncertainties

1. Introduction

1.1 Soil stabilization with T-shaped deep cement mixing piles

Soil stabilization with a cementitious mixture (refers to as deep cement mixing, DCM pile) is frequently used for soft soils treatment before constructing the transport infrastructures, particularly for the roadway embankments [1–6]. Generally, DCM piles are used as a reinforcing volume with a constant circular diameter for entire length of soft soil layers. They achieve to convey the loads persuaded by structures (e.g., embankments) to stronger soil layers at deeper levels. Previous studies on embankment constructions [1–3, 5, 7–9] showed that DCM piles are successful to reduce the settlements of soft soil foundation. However, due to the difference in stiffness between piles and unimproved surrounding soils, unfavorable differential settlements between piles and adjacent soils were found (e.g., [10, 11]). This differential settlement is classified as an important behavior of piled embankment over soft soils that can cause the high-risks to the transport infrastructures during operating period [12–14]).

In recent decades, the T-shaped deep cement mixing (TDM) piles is an innovative technique that has recently been used to support embankments on soft soils [15, 16]. Unlike the DCM piles whose shapes are slender cylinders with a constant diameter throughout their length, TDM piles have a small diameter at their lower part (pile body) with a larger pile diameter at the upper part (pile head). The double-mixing technique (foldable mixing blades) is employed to construct TDM piles [15, 17]. TDM piles have been used to enhance the bearing capacity and reduce ground settlement, lateral displacement, construction costs, and especially to reduce the differential settlement between the piles and surrounding soil, as proven by several previous studies [15, 16, 18–25]. However, for embankments under service, excessive settlement (total and differential settlements) is still the most undesirable characteristic, which can lead to unexpected serviceability and damage to the embankments. Since the inherent

natural soil variability and complex mixing process of soil–cement mixing (SCM) for piles (DCM and TDM piles), high uncertainties in not only the natural soil properties but also the pile mechanical properties can be found in practice [3, 15, 18, 26]. Then, the strength and modulus values of cored soil–cement specimens sampled from the same project site can vary significantly (e.g., [15, 18]). The performance of structures placed on an improved ground can thus be unsafe or overly conservative if only a deterministic analysis is considered. Therefore, reliability assessments of SCM pile-supported embankments are of great importance and should be performed.

1.2 Previous studies of SCM material on reliability framework

Studies considering the spatial variability of the mechanical properties of soil–cement materials have been reported in the literature (e.g., [27–32]). However, most of these previous studies investigated only the effect of the variability of mechanical properties, mainly the unconfined compressive strength (q_u) and the modulus (E), in tested samples or piles observed in the field. These studies showed that the properties of soil–cement materials have large variations. Few studies have investigated the effect of the variability of soil–cement materials on the stability of field embankments. Al-Naqshabandy and Larsson [33] highlighted the influence of spatial variability in the soft soil and DCM piles on the safety factor of the embankment. Navin and Filz [34] showed that the safety factor of DCM pile-supported embankments obtained through a deterministic analysis is not sufficient for the design of these systems. A reliability analysis is thus imperative at the design stage. Relatively few investigations on reliability-based deformation analysis of embankments supported by DCM piles have been reported. Only the most recent studies by Wijerathna and Liyanapathirana [35, 36] included a reliability assessment of the lateral movement combined with the settlement using different reliability methods. They demonstrated that reliability assessments can help

provide adequate safety levels in terms of the deformation performance. Moreover, the random variable method was sufficient to capture the reliability level of piled embankment systems at the preliminary design stage. However, only the influence of the uncertainty in the DCM pile properties was investigated. Moreover, the differential settlement, which is of great concern for road or railway embankments, was not investigated in these studies.

For TDM piles, which are a relatively new technique, no attempt has been made to investigate the deformation of TDM piled embankments in a reliability framework, even though this method has been shown to be effective in reducing excessive differential settlement compared to DCM piles [20, 22, 23]. Furthermore, on the basis of volume control (representing the material cost), the deformation and performance of the embankments also depend on the TDM pile shape (i.e., the sizes of the cap and body) [21–23]. Thus, it is of interest to consider the pile shape during reliability-based deformation analyses to highlight the advantages of using TDM piles.

1.3 Objective of this study

The goal of this work is to apply the reliability framework into the piled embankment systems supported by the TDM piles which is relatively new kind of DCM pile for comprehensive investigation on serviceability behavior, especially for vertical displacements. The study employs the finite element analysis in the framework of two-dimensional axisymmetric numerical modeling to investigate the effect of material uncertainties on the behavior of differential and maximum settlements which is important to the serviceability of piled embankment systems. Reliability-based analysis based on random variable method conducted in this study focuses the long-term behavior of settlements that correspond to a consolidation degree of at least 90% and simultaneously considers the uncertainties in the mechanical properties of the soil, embankment fill, and the pile, as well as the effect of the pile

shape. The uncertainties of strength parameters for soil and pile are correlated to the deformation parameters through empirical equations. The influences of the variabilities of these materials on the differential and maximum settlements of TDM piled embankment systems are discussed and highlighted. To reflect the influence of the TDM pile shape, various cap sizes are considered under an equivalent pile volume. Both individual and system failure modes are considered. A direct coupling analysis between the mechanical model (finite element modeling) and a reliability algorithm (MATLAB software) is considered to avoid manual operations during the probabilistic analysis. A metamodel is used to perform the Monte Carlo simulation (MCS). This is constructed using the Kriging theory combined with an adaptive experimental design algorithm. The performance of TDM piled embankments is evaluated based on the failure probability (P_f), and a reliability analysis of DCM piled embankments is also performed for comparison. The effects of the coefficient of variation (COV) and mean (μ) values on the system are investigated. Note that the failure probabilities in terms of lateral responses of piled embankment systems such as lateral movements and stability embankments are not taken into consideration.

2. Incorporated assumptions and reliability analysis method

2.1 Type and method of the reliability analysis

In a reliability analysis, the methods used to account for the uncertainty in the soil properties can be broadly classified as two types: the random variable method (RVM) and the random field method (RFM). It has been established that the RFM can more effectively represent the uncertainty of soil properties than the RVM (e.g., [37]), particularly when the spatial variability must be considered. However, a high computational effort is required and the discretization effect for different RFM generations should be investigated. For a preliminary design stage considering a reliability assessment of DCM piled embankments, the

RVM is sufficient [36], and no spatial variability is considered. The advantages of the RVM are that it is simpler than the RFM and allows results to be obtained more rapidly [36–39]. Therefore, for the sake of simplicity, the uncertainties of parameters of the soft soil, SCM material, and embankment fill are considered as random variables in the TDM and DCM piled embankment systems in this study.

For reliability analyses, MCS is usually considered the most robust method and is used as a benchmark to check the accuracy of the predicted results (i.e., P_f) obtained with other methods [38, 40]. Nevertheless, when the value of P_f is relatively small ($P_f < 10^{-4}$), reliability analysis using MCS requires very high computational effort and is time consuming, particularly if high accuracy (e.g., a small COV of P_f) is required [41, 42]. For this reason, it is imperative to use improved methods to estimate P_f that can consider a reduced number of iterations of the computational model. Recently, several metamodeling techniques have been developed for reliability analyses of engineering problems, such as artificial neural networks, Kriging, support vector machines, and polynomial chaos expansions. Among these methods, the Kriging metamodeling technique in combination with MCS, proposed by Echard et al. [43] and referred to as the Adaptive Kriging Monte Carlo simulation (AK-MCS), has been recommended [41, 44, 45]. The AK-MCS method can efficiently estimate P_f by constructing a metamodel based on a relatively small number of deterministic simulations. The AK-MCS method demonstrates high efficiency and can accurately provide P_f with a smaller number of iterations of the computational model than the MCS method. Recently, this method has been employed with good performance for reliability analyses of strip footings [41, 44], offshore monopile foundations [45], tunnels [46], and earth dams [39]. Therefore, AK-MCS is the reliability method selected to investigate the P_f of TDM and DCM piled embankments on soft soils presented in this study.

2.2 Random variables

Because the deformation parameters of soils and SCM materials can be correlated with their strength, their uncertainties are usually represented by the strength parameter. For soils, the soil strength ($s_{u,\text{soil}}$) becomes the primary variable using these correlations. The details of these correlations are presented in **Section 3.3**. In the same fashion, the value of the pile modulus (E') was determined to be proportional to the value of the unconfined compressive strength of the pile ($q_{u,\text{pile}}$) as $E' = 100 q_{u,\text{pile}}$ based on the empirical correlation reported in the literature (e.g., [1, 4, 5, 21, 26, 36, 47, 48]). According to several previous studies, c_u of the pile can be derived using $c_u = 0.5 q_{u,\text{pile}}$ (e.g., [3, 5, 36]). For the embankment fill, the stiffness is relatively high owing to the field compaction and the small contribution of the deformation of the fill layer to settlement of the embankment in the service stage. The embankment fill is present to apply the load on the improved soil. The embankment fill unit weight (γ_{emb}) parameter is thus chosen for analysis.

Based on previous studies [32, 33, 35, 36, 49], these three parameters, $s_{u,\text{soil}}$, $q_{u,\text{pile}}$, and γ_{emb} are frequently used in reliability analyses of DCM piled embankments. These three properties are assumed to be uncorrelated and are considered simultaneously in the reliability analyses. All of the random variables are assumed to follow a log-normal probability law. This law avoids generating negative values of the random variables [33, 35, 36]. The details of the three random variables used in the current study are listed in **Table 1**.

2.3 Performance function for the reliability analysis

A performance function, $G(x)$, is used to define a criterion for assessing an unexpected performance of the piled embankments considered in this study. This function is used to

classify the limit state surface separating the failure and safety domains, where x represents a random vector of the input random variables. Normally, the limit state surface can be defined mathematically as $G(x)=0$, where $G(x)<0$ represents the failure domain, and $G(x)>0$ represents the safety domain. Regarding the settlement reliability of piled embankments (i.e., the serviceability limit state (SLS) requirements), two performance functions have been adopted in the current study. The function for the differential settlement is defined as follows:

$$G_1(x)=\Delta s^a-\Delta s \tag{1}$$

The second function for the maximum settlement can be expressed as follows:

$$G_2(x)=s_{\max}^a-s_{\max} \tag{2}$$

where Δs^a and $s_{\max}^a$ are the allowable differential and maximum settlements, respectively, which are detailed in **Section 4**. The differential settlement is defined as the difference in settlements between pile head settlement (point C, see **Fig. 1**) and surrounding soil settlement (point D, see **Fig. 1**) while the maximum settlement is defined as the average settlement occurred on the top slab (line AB, see **Fig. 1**).

Fig. 1 Layout of the simulated unit cell: (a) plan; (b) elevation view of the DCM piled embankment; and (c) elevation view of the TDM piled embankment

Using MCS with N_{MCS} runs of the computational model, the failure probability, P_f, can be calculated as follows:

$$\mathrm{P}_f=\frac{1}{N_{MCS}}\times\sum_{i=1}^{N_{MCS}}I_{MCS} \tag{3}$$

where I_{MCS} is an indicator of failure; I_{MCS} is equal to 1 if the system fails ($G(x)<0$) and I_{MCS} = 0 otherwise. N_{MCS} is the total number of MCS samples; N_{MCS} should be large enough to

obtain an accurate P_f with a small value of the coefficient of variation for P_f (COV-P_f). COV-P_f can be estimated as follows:

$$\text{COV-P}_f = \sqrt{\frac{1-\text{P}_f}{N_{MCS} \times \text{P}_f}} \times 100\% \quad (4)$$

Taking into account the SLS requirements, the three random variables mentioned above are adopted in this study for the criteria of both the differential (P_f^{diff}) and maximum (P_f^{max}) settlements. Another failure mode is the system failure probability (P_f^{sys}) of the piled embankment addressed herein, which is satisfied if any individual failure criterion exceeds the allowable value [38].

2.4 Adaptive Kriging Monte Carlo simulation (AK-MCS)

To estimate P_f, AK-MCS is used for the reliability analysis. This method is an active learning reliability method comprising the combination of a Kriging metamodel and MCS, as proposed by Echard et al. [43]. The AK-MCS method is based on the Kriging theory, which guarantees the construction of a metamodel with high accuracy in the vicinity of the limit state surface. Using this method, it is possible to estimate the failure probability, P_f, by generating a small number of realizations of the metamodel (i.e., analytical function) instead of the large number required for computational models (i.e., finite element models). In this method, a small number of samples (designs of experiments, DoE) are used to construct the Kriging metamodel in the initial stage (e.g., a dozen samples have been used [43]). Then, this metamodel is updated by adding a new sample in each iteration following the conditions of a powerful learning function. This procedure is repeated until an imposed stopping condition is achieved. To choose the next candidate for the new sample with the highest probability, the U-function expressed in **Eq. (5)** is used as the powerful learning function:

$$U(x)=\frac{|\mu_G(x)|}{\sigma_G(x)} \tag{5}$$

where $\mu_G(x)$ and $\sigma_G(x)$ are the mean and standard deviation values of the Kriging predictions, respectively. To end the adjustment process for the Kriging model, the stopping criterion proposed by Schöbi et al. [50] is employed, which only considers the uncertainty of the P_f estimation:

$$\frac{P_f^+ - P_f^-}{P_f^0} \le \varepsilon_{P_f} \tag{6}$$

where P_f^0 is the mean estimation of the Kriging model, $\mu_G(x)$, used to identify I_{MCS} ($P_f^0 = P(\mu_G(x) \le 0)$); P_f^+ is the upper bound failure probability ($P_f^+ = P(\mu_G(x) + k\sigma_G(x) \le 0)$); and P_f^- is the lower bound failure probability ($P_f^- = P(\mu_G(x) - k\sigma_G(x) \le 0)$). A k value of 1.96 is selected based on a previous study [50]. In this study, the AK-MCS ends when the error estimation of the failure probability (ε_{P_f}) is less than 5%. This criterion value seems acceptable, as suggested and detailed by Schöbi et al. [50] and Guo and Dias [39].

2.5 Computational framework

In this study, the calculation of failure probabilities is facilitated by the UQLab software package [51]. The UQLab software is implemented within MATLAB and can be connected to the PLAXIS finite element software. A personal computer equipped with an Intel Core i7 running at 4.0 GHz and having 16 GB of RAM is used for the computations.

3. Deterministic analysis of piled embankments

3.1 Reference piled embankment cases

Embankments supported by DCM or TDM piles are used as reference cases to construct the reliability analyses. A geological profile composed of a homogeneous soft clay layer with a thickness of 10 m is considered. This layer is situated above a nondeformable substratum. A 1.5-m-high embankment fill (weathered clay) is placed on top of the pile–improved subsoil foundation. A 0.2-m-thick concrete slab is located on top of the embankment fill to apply the loading. The ground water table is set at the original ground surface. Two different pile types, DCM and TDM piles, are chosen in the present study under the condition of a controlled pile volume. The reference DCM pile with a diameter (D_{DCM}) of 0.8 m and a pile length (L_{DCM}) of 6 m is selected based on the prototype case in a previous study [23]. Based on the past studies, a TDM pile with shape factor (α_s) of at least 3.0 is recommended to ensure the effectiveness of enlarging the pile caps for reducing the differential settlement [22] and improving of the pile capacity [21] compared with DCM piles under the same volume. The α_s parameter represents the ratio of the bearing area of the TDM pile to that of the DCM pile over the ratio of the skin area of the TDM pile to that of the DCM pile, as given by the following [21]:

$$\alpha_s = \frac{D_{TDM}^2 / D_{DCM}^2}{\left[\left(D_{TDM} - d_{TDM}\right)H + d_{TDM}L_{TDM}\right] / D_{DCM}L_{DCM}} \tag{7}$$

where D_{TDM} is the pile head diameter of the TDM pile, d_{TDM} is the pile body diameter of the TDM pile, H is the thickness of the enlarged pile cap of the TDM pile, and L_{TDM} is the TDM pile length.

Consequently, a TDM pile with an α_s of 3.0 is chosen for this study as an additional reference case. A d_{TDM} of 0.5 m is selected based on previous studies [15, 18, 21, 22], and L_{TDM} is set as equal to L_{DCM}. Accordingly, D_{TDM} and H are equal to 1.31 m and 1.6 m, respectively. The piles are arranged in a square grid pattern with a center-to-center spacing (S) of 2.0 m, corresponding to an area improvement ratio (a_r) of 12.6% for the DCM pile case

and 33.7% for the TDM pile case. This a_r ratio falls within the range of 10–50% commonly used in engineering [5, 15, 16]. Based on the literature review, the unconfined compressive strength of SCM piles is in the range of 200–2700 kPa [3, 5, 15, 18, 52]. The minimum SCM pile strength value of 200 kPa is selected for both cases (DCM and TDM piles). Considering the symmetry condition, it is possible to investigate the settlement behavior of the pile–embankment system using a two-dimensional axisymmetric model (see **Fig. 1(b)** and **1(c)**) with an equivalent diameter of $1.128S$, as presented in **Fig. 1(a)**. This modeling approach can provide results with good accuracy compared to three-dimensional modeling, while requiring less computational time [23, 53]. The problem is modeled as a single pile in a network situated far from the embankment slope. **Fig. 1(b)** and **1(c)** also depict points A–D, which are used to monitor the settlement behavior of the piled embankment systems. Points A and B are located at the concrete slab crest, whereas points C and D are positioned at the ground surface. Line AB is chosen to investigate the maximum settlement, while line CD is selected for monitoring the differential settlement between the pile and the surrounding soil.

3.2 Numerical modeling

Two-dimensional axisymmetric numerical calculations were conducted using the PLAXIS 2D finite element modeling program [54] to analyze the piled embankment systems. Fifteen-node triangle elements were used for the mesh generation. A perfect bonding between the soft soil and SCM piles was adopted for this study because the shear strength at the interface between the SCM piles and the surrounding soil is greater than the soil shear strength, as commonly used in previous studies (e.g., [5, 8, 22]). FE analyses were carried out to simulate the consolidation behavior after finishing embankment construction using a coupled mechanical and hydraulic modeling that permitting a dissipation of excess pore pressures in the saturated clays as a function of time. A constant surcharge load of 25 kPa over the concrete

slab was applied to consider the settlement behavior with an elapsed time of 1500 d, corresponding to consolidation degree of not less than 90%. The simulation details for the piled embankment system are summarized in **Table 2**. **Fig. 2** shows an example of the FE mesh used in this study. The bottom boundary of the finite element (FE) mesh was fixed in all directions because the soft soil layer was placed on the rigid substratum, while the top boundary was left free. The lateral boundaries were constrained in the normal direction. Water could drain freely at the ground surface and the bottom boundary.

Fig. 2 Mesh of the piled embankment

3.3 Constitutive models and model parameters

In this study, the constitutive models and model parameters for the soft soil, SCM pile, and embankment fill were adopted from a previous study by Phutthananon et al. [22]. These parameter sets were well calibrated based on the oedometer and triaxial testing results for soil samples obtained from the actual site of a DCM piled embankment. Moreover, the simulated results for the DCM piled embankment were also validated based on monitoring data, and good agreement was obtained. A more detailed description of the calibration and validation are provided in the literature [22].

3.3.1 Soft soil

To model the soft soil behavior, the Hardening Soil (HS) model [55] was chosen. According to previous studies, the HS model is effective for predicting the deformation of soft soils [21, 22, 26, 56–59]. The set of soft soil material parameters for the HS model was adopted from Phutthananon et al. [22], as listed in **Table 3**. The HS model parameters can be divided into two main groups: shear strength parameters and deformation parameters. The shear

strength parameters based on the Mohr–Coulomb shear criterion include the effective cohesion (c'), effective friction angle (ϕ'), and dilatancy angle (ψ'). Five basic deformation parameters were used for the HS model: the reference secant stiffness in standard drained triaxial tests (E_{50}^{ref}), reference tangential stiffness for a primary oedometer loading (E_{oed}^{ref}), reference unloading/reloading stiffness (E_{ur}^{ref}), Poisson's ratio for unloading/reloading ($\nu_{ur} = 0.2$ was used in this study [54]), and power of the stress-level dependency of the stiffness ($m = 1$ was suggested by Surarak et al. [59] for soft clayey soils). A value of $E_{50}^{ref} = 160 s_{u,\,\mathrm{soil}}$ was considered in this study. This relationship falls within the range of $60 s_{u,\,\mathrm{soil}} - 330 s_{u,\,\mathrm{soil}}$ used in several previous studies [21, 60, 61]. E_{oed}^{ref} and E_{ur}^{ref} were estimated as $E_{oed}^{ref} = E_{50}^{ref}$ and $E_{ur}^{ref} = 3E_{50}^{ref}$, respectively, as generally used in other works [8, 61–63]. Procedures similar those recommended by Jamsawang et al. [56] were adopted to determine the input HS model parameters; the calibration results for those parameters can be found in Phutthananon et al. [22].

3.3.2 SCM pile, embankment fill, and concrete slab

The SCM pile and embankment fill were modeled using linear elastic–perfectly plastic behavior with the Mohr–Coulomb failure criterion (named the MC model). This model has been successfully used to simulate the behavior of SCM piles and the embankment fill in the literature [3–5, 8, 12, 64–67]. In the present study, sets of material parameters for the SCM pile and embankment fill were adopted from the work of Phutthananon et al. [22]. **Table 4** lists the input parameters for the MC model used in this study. For the input parameters of the SCM pile, the available procedure in PLAXIS, i.e., Undrained (B), was chosen for the analyses by using the effective elastic modulus (E') and undrained shear strength (c_u) [5, 22, 54]. The concrete slab was considered to be linear elastic (LE) with a unit weight (γ) of 25 kN/m^3,

Young's modulus (E) of 10 GPa, and Poisson's ratio (ν) of 0.20. It should be noted that although the coefficients of permeability of SCM piles adopted in this study are relatively high; they have insignificant effect on the computed settlement results discussed herein because the consolidation analyses are performed until the consolidation degree of not less than 90% is achieved.

4. Settlement of the reference embankment cases using deterministic analysis

In this section, the behaviors of the embankments improved by DCM and TDM piles described in **Section 3.1** are analyzed by assuming deterministic properties for all of the materials listed in **Tables 3** and **4**. **Fig. 3** presents the results for the vertical stresses acting on the pile head and surrounding soil for both reference cases. As expected for both cases, the vertical stress acting on the surrounding soil is lower than that acting on the pile head. This can be attributed to the arching effect caused by the different moduli between the pile and the soil, as described in previous publications [16, 19]. Comparing the results for the DCM and TDM piles reveals that the induced vertical stresses on the TDM pile head are lower than those on the DCM pile head. This is caused by the larger cross-sectional area of the TDM pile head (higher value of a_r), as noted in previous studies [16, 20, 22].

Fig. 3 Stress distribution along line CD for the reference DCM and TDM piled embankments

The changes in the settlement distribution inside the embankment fill and slab for both cases are depicted in **Fig. 4**. Large settlements are found at the slab top, which then decay from the slab top to the ground surface. For both cases, settlement arches are formed above the pile head and are approximately dome-shaped. The boundaries of the settlement arches are very close to the pile edge. The arch height above the DCM pile is higher than that above the TDM

pile. As can be seen, the minimum settlements occur in the vicinity of the pile heads. A comparison of the pile types shows that the piled embankment system with DCM piles provides less settlement at both the slab top and ground surface. The settlements at the top of the slab (AB line, see **Fig. 1**) and ground level (CD line, see **Fig. 1**) are plotted in **Fig. 5**. Under the same loading and pile volume conditions, the settlements of the TDM piled embankment at both positions are greater than those of the DCM piled embankment. The maximum settlement (s_{max}, the average settlement of the slab top) of the TDM piled embankment is 303.60 mm, while s_{max} = 228.92 mm for the DCM piled embankment. This trend is in good agreement with the computed results for embankments supported by DCM and TDM piles reported by Phutthananon et al. [22]. This can be explained by the fact that a greater portion of the embankment load is applied to the TDM piles owing to the larger pile head [15, 16, 20]. Once large settlements occur in the piles themselves, they can no longer inhibit the settlement of the surrounding soil, resulting in large soil settlements [22]. However, when considering the differential settlements (Δs) in these two cases, the TDM piled embankment can provide a markedly lower Δs compared with the DCM piled embankment. A Δs value of 12.95 mm is obtained for the TDM piled embankment, whereas the Δs for the DCM piled embankment is 44.41 mm. Interestingly, the use of TDM pile-supported embankments can reduce Δs by approximately 70% compared to the use of DCM piles. This result is in good agreement with the results of physical model tests reported by Yi et al. [16] and Phutthananon et al. [22] and numerical simulations reported by Yi et al. [20] and Phutthananon et al. [22]. Therefore, in this study, the values of Δs = 12.95 mm and s_{max} = 303.60 mm obtained from the TDM piled embankment (α_s = 3) were defined as the allowable differential and maximum settlements, respectively, in the reliability analysis in the following section.

Fig. 4 Settlements within the embankment fill and slab for different piled embankments: (a) settlement in the reference DCM piled embankment; and (b) settlement in the reference TDM piled embankment

Fig. 5 Settlements in the reference DCM and TDM piled embankments: (a) settlement along line AB (at the top of the slab); and (b) settlement along line CD (at the ground surface)

5. Reliability analysis results

5.1 Validation of the reliability results provided by AK-MCS

Although the AK-MCS method is robust and not very time-consuming [41, 44, 45], it is necessary to evaluate the accuracy of the P_f estimation obtained with this method. To this end, the P_f estimated using direct MCS is adopted as the benchmark. **Fig. 6** illustrates the P_f^{diff} for the reference TDM piled embankment case computed using direct MCS with various number of samples. The result obtained using AK-MCS is also included. It can be seen that the direct MCS results provide an estimated P_f^{diff} of 0.413 with a coefficient of variation of P_f, COV-P_f, of approximately 2.18% after approximately 3000 realizations. The estimated P_f^{diff} provided by the AK-MCS method is 0.416, which is very close to the result obtained with the direct MCS. Moreover, the COV-P_f obtained with the AK-MCS is very low compared with that of the direct MCS (0.37% << 2.18%). These results indicate that the constructed metamodel based on Kriging theory is efficient for estimating the settlement values of piled embankment systems and thus providing reliability analysis results. Hence, by adopting the AK-MCS method in this study, the failure probability can be estimated with reasonable accuracy.

Fig. 6 Comparison of the differential settlement failure probabilities (P_f^{diff}) for the reference TDM piled embankment case obtained with the direct MCS and AK-MCS reliability methods

5.2 Influence of the pile shape

An important independent variable in the design of TDM piled embankments is the pile shape factor, α_s, which is the significant parameter for controlling the ultimate bearing capacity and settlement of TDM piled embankments over soft soils [21, 22]. To investigate the effect of this factor on the failure probability while also considering the cost effectiveness, α_s is varied based on the condition of a controlled pile volume of the DCM pile (D_{DCM} = 0.8 m and L_{DCM} = 6.0 m). The TDM pile length (L_{TDM}) and pile body diameter (d_{TDM}) are kept constant and are 6.0 m and 0.5 m, respectively. TDM pile head diameters are considered in the range of 1.0–1.5 m, which corresponds to thicknesses of the enlarged pile cap in the range of 1.17–3.12 m. The pile shapes adopted in this study were carefully selected considering the available dimensions used in practice [5, 15, 18–23]. Hence, the reliability analyses are conducted for values of α_s = 1.0, 1.6, 2.2, 3.0, 3.5, and 4.0. The detailed configurations of these pile shapes are presented in **Table 5**.

The results obtained with AK-MCS for the two limit state functions described above are displayed in **Fig. 7**. Three failure probabilities, P_f^{diff}, P_f^{max}, and P_f^{sys}, are plotted in this figure. Three random variables (i.e., $s_{u,\,soil}$, $q_{u,\,pile}$, and γ_{emb}) are considered simultaneously to investigate the failure probabilities by considering the mean (μ) values and coefficient of variation of mean (COV-μ) values, as listed in **Table 1**. As seen in **Fig. 7**, P_f^{diff} does not change significantly when α_s increases from 1.0 to 2.2 (small TDM piles with thicker pile caps). However, it is evident that P_f^{diff} decreases considerably with increasing α_s of greater than 2.2

(larger TDM piles with thinner pile caps). Interestingly, the use of TDM piles with α_s = 4.0 can decrease P_f^{diff} by approximately 99% relative to the DCM pile case (α_s = 1.0). This result is attributed to the larger pile head diameter, which can increase the load transfer to the piles through arching effects [5, 15]. Hence, a large pile settlement and small soil settlement are obtained, resulting in a decrease in the differential settlement [22]. This is in good agreement with the numerical results reported by Yi et al. [20]. In contrast, an increase in α_s leads to an increase in P_f^{max}. In the studied range, P_f^{max} for the case of TDM piles with α_s = 4.0 (P_f^{max} = 0.572) is approximately 1.26 times greater than that for α_s = 1.0 (DCM pile, P_f^{max} = 0.455). Again, this result is attributed to the enlarged pile cap of the TDM pile, as described previously in **Section 4**. This tendency is in good agreement with the computational results for embankments supported by TDM and DCM piles obtained by Phutthananon et al. [22]. Inspecting the results for P_f^{sys} reveals that the use of TDM piles can reduce P_f^{sys} dramatically compared to the use of DCM piles, particularly when α_s is in the range of 2.2 to 4.0. Using TDM piles with α_s = 4.0 can drastically reduce the value of P_f^{sys} from 0.99 (for the case of DCM piles) to 0.58. Based on these results, it can be concluded that the decrease of P_f^{sys} is mainly governed by the variation in P_f^{diff}. It is also noted that the decrease in P_f^{sys} is not as great as that of P_f^{diff} owing to the inclusion of P_f^{max}, which has a relatively large value. However, the rate of increase in P_f^{max} is much smaller than the rate of decrease in P_f^{diff}. Consequently, TDM piles with large heads can provide very low values of P_f^{sys} compared to those for DCM piles. This result is due to the fact that DCM piles induce a large value of P_f^{diff} (up to 0.94 in this study). The results of this study present a promising alternative of using TDM piles to support

embankments on soft soils with a high degree of safety. The use of this pile type can effectively avoid undesired performance of the embankment in terms of serviceability (i.e., settlement).

Fig. 7 Impact of the pile shape factor (α_s) on the differential settlement (P_f^{diff}), maximum settlement (P_f^{max}), and system (P_f^{sys}) failure probabilities of the piled embankment

6. Parametric studies

To investigate the effect of each random variable on the computed system failure probabilities, P_f^{sys} of the embankments supported by TDM and DCM piles, parametric analyses were performed. The mean (μ) and coefficient of variation of mean (COV-μ) values for each random variable were varied in the reliability analysis, as listed in **Table 6**.

6.1 Impact of the uncertainties of soft soil properties

The parametric analyses of the SCM piled embankment in this subsection aim to assess the impact of the variability in the μ-$s_{u,\,soil}$ and COV-$s_{u,\,soil}$ values (soft soil parameters) on the estimated reliability results. The values of μ-$s_{u,\,soil}$ for very soft soils and soft soils are considered to be in the range of 5–10 kPa and 15–25 kPa, respectively [68, 69]. The ranges of the COV-$s_{u,\,soil}$ values are adopted from Phoon and Kulhawy [70].

The variation between the μ-$s_{u,\,soil}$ and the P_f^{sys} of the embankments supported by SCM piles for different α_s values, is shown in **Fig. 8**. For the case of small α_s values, the P_f^{sys} value decreases slightly with increasing μ-$s_{u,\,soil}$. For example, for α_s = 1.0 (DCM pile), the value of P_f^{sys} declines from 1 to 0.935 with the increase in μ-$s_{u,\,soil}$ from 5 to 25 kPa. A similar trend is also observed for α_s = 1.6 and 2.2 (small TDM piles with larger caps). When α_s exceeds

2.2, the P_f^{sys} value decreases substantially with increasing μ-$s_{u,\,soil}$. For instance, in the case of α_s = 4.0 (TDM pile with a large but thin cap), the value of P_f^{sys} decreases from 1 to 0.074 as μ-$s_{u,\,soil}$ increases from 5 to 25 kPa. Interestingly, increasing μ-$s_{u,\,soil}$ from 10 to 25 kPa can dramatically reduce P_f^{sys} by approximately 92%. From these results, it can be concluded that the use of DCM and TDM piles to support embankments on very soft soils (i.e., $s_{u,\,soil}$ = 5–10 kPa) does not significantly change the reliability level (i.e., P_f^{sys}). This result is attributed to the difference in stiffness between the soil and pile materials, as revealed by previous studies on DCM piles [7] and TDM piles [22]. For this reason, unacceptably high failure probabilities (large P_f^{sys}) are obtained for SCM piled embankments over very soft soils regardless of the pile shape. However, when using this improvement system on soft soils (i.e., $s_{u,\,soil}$ = 15–25 kPa), it is evident that the use of TDM piles (especially for cases where α_s exceeds 3.0) can effectively provide good reliability levels (small P_f^{sys}) compared to the use of DCM piles. Interestingly, the deterministic analysis [22] also reveals that the use of TDM piles with α_s of greater than 3.0 can significantly reduce the differential settlement. As a result, the confidence level of embankments supported by TDM piles can be increased. This finding suggests that the use of TDM piles with large heads can significantly reduce the occurrence of undesired settlement.

Fig. 8 Impact of the mean value of $s_{u,\,soil}$ (μ-$s_{u,\,soil}$) in association with the pile shape factor (α_s) on the system failure probability (P_f^{sys})

Fig. 9 presents P_f^{sys} as a function of the COV-$s_{u,\,soil}$ values in association with α_s. The results show that the influence of COV-$s_{u,\,soil}$ on P_f^{sys} is almost insignificant. P_f^{sys} decreases slightly with increasing COV-$s_{u,\,soil}$ with α_s ranging from 1.0 to 2.2, i.e., the P_f^{sys} value at COV-$s_{u,\,soil}$ = 0.44 decreases by approximately 1% compared that at COV-$s_{u,\,soil}$ = 0.04. Beyond that (α_s = 3.0–3.5), the value of P_f^{sys} gradually increases with increasing COV-$s_{u,\,soil}$. For the case of α_s = 4.0, it appears that the magnitude of P_f^{sys} becomes almost constant with varying COV-$s_{u,\,soil}$. Therefore, it can be concluded that COV-$s_{u,\,soil}$ has a slight impact on the reliability of SCM piled embankments in terms of P_f^{sys}.

Fig. 9 Impact of the coefficient of variation of $s_{u,\,soil}$ (COV-$s_{u,\,soil}$) in association with the pile shape factor (α_s) on the system failure probability (P_f^{sys})

6.2 Impact of the uncertainties of SCM pile properties

The effect of μ-$q_{u,\,pile}$ on P_f^{sys} is investigated in this section. The values of μ-$q_{u,\,pile}$ range from 200–800 kPa, as is frequently used in practice [4, 26, 35, 36, 60].

The variation in the value of P_f^{sys} with changing μ-$q_{u,\,pile}$ is presented in **Fig. 10**. It is evident that for all values of μ-$q_{u,\,pile}$, P_f^{sys} decreases with increasing α_s, particularly for the cases of TDM piles with large caps (high α_s). The change in P_f^{sys} with varying μ-$q_{u,\,pile}$ for the same α_s shows that μ-$q_{u,\,pile}$ has a negligible effect on the change in P_f^{sys} when α_s is less than 2.2. In other words, the use of TDM piles with small pile caps cannot enhance the reliability or suppress the excessive settlement of the piled embankment within the range of μ-$q_{u,\,pile}$ values used in this study. When α_s is equal to 3.0, P_f^{sys} increases with increasing μ-$q_{u,\,pile}$. As can be

seen, the value of P_f^{sys} can be increased from 0.863 to 0.983 with the increase in μ-$q_{u,\text{pile}}$ from 200 to 800 kPa. This increasing trend is similar to the results for the case of α_s = 3.5. This result is not surprising as a high $q_{u,\text{pile}}$ can restrain the large pile settlement, consequently producing a large differential settlement [22] and resulting in an increase in P_f^{sys}. For the data set with α_s = 4.0, the magnitude of P_f^{sys} gradually decreases from 0.579 to 0.517 until μ-$q_{u,\text{pile}}$ reaches 400 kPa. Beyond that, P_f^{sys} continues to increase with μ-$q_{u,\text{pile}}$ up to 800 kPa (P_f^{sys} = 0.690). Interestingly, the use of TDM piles with α_s = 4.0 for μ-$q_{u,\text{pile}}$ = 800 kPa can reduce P_f^{sys} by approximately 30% compared with using DCM piles at the same μ-$q_{u,\text{pile}}$. From these results, it can be concluded that both the pile strength ($q_{u,\text{pile}}$) and enlarged pile cap shape (α_s) play an important role in the reliability of SCM piled embankments, especially for large α_s values. To ensure the effective enhancement of the reliability level, pile shapes with α_s values of greater than 3 are recommended for all of the $q_{u,\text{pile}}$ values used in this study. Moreover, it is also possible to use TDM piles with large caps (α_s > 3) at high values of q_u to increase the reliability level of SCM piled embankments or to avoid excessive settlement of the overlying structure. This solution is very promising for soft soil improvement when the embankment is required to support a super-structure (i.e., a high $q_{u,\text{pile}}$ is needed).

Fig. 10 Impact of the mean value of $q_{u,\text{pile}}$ (μ-$q_{u,\text{pile}}$) in association with the pile shape factor (α_s) on the system failure probability (P_f^{sys})

Fig. 11 illustrates the estimated P_f^{sys} with varying COV-$q_{u,\text{pile}}$ for different values of α_s. The values of COV-$q_{u,\text{pile}}$ considered in this study are adopted from the previous study by

Wijerathna and Liyanapathirana [36]. Under the same COV-$q_{u,\text{pile}}$, the P_f^{sys} values initially decrease gradually (α_s in the range of 1.0–2.2) and then rapidly approach a P_f^{sys} of less than 0.6 when α_s reaches 4.0. For the change in P_f^{sys} with identical values of α_s, the magnitude of P_f^{sys} slightly decreases with increasing COV-$q_{u,\text{pile}}$ for α_s in the range of 1.0–3.0. The highest degree of decrease in P_f^{sys} is approximately equal to 4%, which occurs with the change in COV-$q_{u,\text{pile}}$ value from 0.3 to 0.7. This result is obtained with α_s = 1.6. As the α_s value increases (i.e., α_s = 3.5 and 4.0), the magnitude of P_f^{sys} exhibits the opposite trend. For instance, the magnitude of P_f^{sys} increases by approximately 6% with the change in COV-$q_{u,\text{pile}}$ from 0.3 to 0.7. These results imply that the influence of COV-$q_{u,\text{pile}}$ on the reliability of SCM piled embankments is insignificant. Moreover, it seems that the influence of COV-$q_{u,\text{pile}}$ on the reliability level is less than that of μ-$q_{u,\text{pile}}$ presented above. Therefore, in the reliability analysis of SCM piled embankments in terms of the system failure modes (considering both the differential and maximum settlements), the effect of COV-$q_{u,\text{pile}}$ can be ignored.

Fig. 11 Impact of the coefficient of variation of $q_{u,\text{pile}}$ (COV-$q_{u,\text{pile}}$) in association with the pile shape factor (α_s) on the system failure probability (P_f^{sys})

6.3 Impact of the uncertainties of embankment fill properties

For a better understanding of the effect of the uncertainty of γ_{emb} on P_f^{sys}, the μ-γ_{emb} and COV-γ_{emb} values are varied here in association with α_s. The ranges of μ-γ_{emb} and COV-γ_{emb} values reported by Phoon and Kulhawy [70] are applied in this study.

Fig. 12 displays the variation between P_f^{sys} and μ-γ_{emb} for different values of α_s. The results with the same values of μ-γ_{emb} indicate that the value of P_f^{sys} remains almost constant with an increase in α_s from 1.0 to 2.2 and then rapidly decreases with further increases in α_s. For example, for μ-γ_{emb} = 14 kPa, P_f^{sys} decreases from 1 to 0.398 with the increase in α_s from 2.2 to 4.0. In this range, the P_f^{sys} value decreases by approximately 60%. This is because the use of TDM piles with large caps can significantly reduce the differential settlement [22]. Hence, lower P_f^{sys} values can be obtained with large α_s. Investigating the variability of μ-γ_{emb} reveals that μ-γ_{emb} has a slight effect on P_f^{sys} for small α_s (DCM piles and small TDM piles with thicker pile caps). However, μ-γ_{emb} has an important impact on P_f^{sys} when α_s is in the range of 3.0 to 4.0 (TDM piles with large but thin caps). In this range, a decrease in μ-γ_{emb} leads to a substantial decrease in P_f^{sys}. For α_s = 4.0, P_f^{sys} decreases drastically from 0.850 to 0.398 as μ-γ_{emb} decreases from 20 to 14 kN/m^3. This may be attributed to the decrease in the applied load above the pile–soil system as a result of the reduction in μ-γ_{emb}. This phenomenon leads to reduction of the settlement [5, 9]. From the results in this study, it is promising to recommend that TDM piles with large heads (high α_s) can be used to provide a high reliability of piled embankments compared to that of DCM piles with the same pile volume.

Fig. 12 Impact of the mean value of γ_{emb} (μ-γ_{emb}) in association with the pile shape factor (α_s) on the system failure probability (P_f^{sys})

Fig. 13 presents the distribution of P_f^{sys} for three different values of COV-γ_{emb} and six different pile shapes. The results show that the value of P_f^{sys} decreases with increasing α_s. It is

clear that P_f^{sys} for $\alpha_s = 4.0$ is approximately 40% smaller than that for $\alpha_s = 1.0$. This reduction is observed for all of the COV-γ_{emb} values considered in this study. Investigating the effect of COV-γ_{emb} reveals that the change in COV-γ_{emb} seems to have an insignificant influence on P_f^{sys} when α_s is in the range of 1.0 to 2.2. When α_s is greater than 2.2, P_f^{sys} decreases slightly with increasing COV-γ_{emb}. For example, for the case of $\alpha_s = 4.0$, P_f^{sys} decreases from 0.586 to 0.553 (a reduction of approximately 6%) when COV-γ_{emb} increases from 0.03 to 0.20. Therefore, it seems that the reliability levels of the SCM piled embankments in term of P_f^{sys} are not significantly affected by COV-γ_{emb}. Moreover, within the ranges of μ-γ_{emb} and COV-γ_{emb} values considered in this study, μ-γ_{emb} has an impact on the reliability level, while COV-γ_{emb} does not. This implies that the reliability-based settlement analysis of the SCM piled embankment is more sensitive to the uncertainty of μ-γ_{emb}. Hence, appropriate values of μ-γ_{emb} should be carefully chosen for reliability-based settlement analyses in the design of SCM piled embankments.

Fig. 13 Impact of the coefficient of variation of γ_{emb} (COV-γ_{emb}) in association with the pile shape factor (α_s) on the system failure probability (P_f^{sys})

7. Discussion

The RVM is employed to simulate the uncertainty of material properties (soft soil, SCM pile, and embankment fill) for SCM piled embankments on soft soils. In the event that a direct MCS method is adopted to conduct the reliability-based settlement analysis for this problem (reference TDM pile case, $P_f^{diff} = 0.420$), at least 750 model calls are required for a target error,

COV-P_f, of less than 5% (COV-P_f = 4.29%), requiring approximately 9.6 h to complete. By applying the framework proposed in this study to the aforementioned TDM piled embankment problem, the AK-MCS method requires a much smaller number of calls of the deterministic model used to construct the metamodel. This is highly significant for reducing the computational time of the reliability analysis. The P_f^{diff} value obtained with the AK-MCS method is 0.416, corresponding to a COV-P_f = 0.37% (much smaller than that obtained with the direct MCS method); moreover, a calculation time of only 0.4 h is required. This indicates that using the AK-MCS method can significantly reduce the computational time by at least 9 h compared to the direct MCS method, while providing reliability results with a higher confidence level. Therefore, the AK-MCS method used in this study for considering the uncertainty of SCM piled embankment systems could serve as a suitable alternative, as it is very efficient.

According to the results presented in **Section 5.2**, the failure probability related to the differential settlement (P_f^{diff}) is mainly controlled by α_s. The piles with large α_s can provide very small values of P_f^{diff}, particularly when α_s is greater than 3.0 (TDM piles with large but thin pile caps). Meanwhile, TDM piles with large caps can induce large failure probabilities for the maximum settlement (P_f^{max}). However, the increase in P_f^{max} with α_s is relatively small when compared to the decrease in P_f^{diff}. For an accurate design, serviceability requirements in terms of the differential and maximum settlement criteria must be taken into account to prevent undesired settlement characteristics. Hence, the system failure probability (P_f^{sys}) introduced in this study is a good indicator for capturing the failure modes in terms of both the differential and maximum settlements. The results presented in **Fig. 7** indicate that compared to DCM piles with the same volume, the use of TDM piles can effectively enhance the reliability level of SCM piled embankments when the uncertainty of materials is taken into account. This finding

is very useful for geotechnical engineering to reduce undesired performance in terms of the settlement of the piled embankment system.

Based on the parametric studies presented in **Section 6**, it is concluded that the mean values of all of the random variables (μ-$s_{u,\,\mathrm{soil}}$, μ-$q_{u,\,\mathrm{pile}}$, and μ-γ_{emb}) have important effects on $\mathrm{P}_f^{\mathrm{sys}}$ when α_s is greater than 2.2 (TDM piles with large caps). Particularly, for α_s of greater than 3, the TDM piles can drastically reduce the influence of the material variability in terms of the μ values on $\mathrm{P}_f^{\mathrm{sys}}$. This is because the TDM piles with large caps can markedly decrease the differential settlement for any value of μ. On the other hand, for the $\mathrm{P}_f^{\mathrm{sys}}$ considered in this study, the impacts of the three coefficients of variation (COV-$s_{u,\,\mathrm{soil}}$, COV-$q_{u,\,\mathrm{pile}}$, and COV-γ_{emb}) are insignificant. However, as an individual failure mode, $\mathrm{P}_f^{\max}$ is still affected by the COV values of all materials. This result is in good agreement with the reliability results obtained by Wijerathna and Liyanapathirana [35, 36], who reported that the variation in COV-$q_{u,\,\mathrm{pile}}$ significantly affected the individual failure probabilities of the maximum settlement and lateral displacement of DCM pile-supported embankments on soft soils.

8. Conclusions

The main conclusions of this study can be drawn as follows:

(1) The AK-MCS method can considerably decrease the computational time required to conduct a reliability analysis with a high confidence level, although the failure probability result is lower. For the preliminary design stage, AK-MCS can be effectively adopted for reliability assessments that require a large number of iterations to computationally expensive mechanical models instead of a more general reliability method (i.e., MCS).

(2) The use of TDM piles with large caps (α_s > 3.0) is recommended to ensure the effectiveness of using TDM piles for the enhancement of the reliability level or reduction

of the system failure probability. These TDM piles can provide significantly lower estimations of the differential settlement failure probability compared to the use of DCM piles. However, the use of TDM piles with large caps should be handled carefully owing to a slight increase in the maximum settlement failure probability.

(3) A high reliability level in terms of the system failure probability can be found for the case of TDM piles with large heads but thinner caps. This promotes the use of TDM piles to reduce the undesired performance of settlement considering all of the material variabilities for piled embankment systems.

(4) The mean values of the materials considered in this study (μ-$s_{u,\,\mathrm{soil}}$, μ-$q_{u,\,\mathrm{pile}}$, and μ-γ_{emb}) are found to have a significant effect on the system failure probability of SCM piled embankments on soft soils. Importantly, these parameters should be carefully selected for consideration in reliability analyses in further investigations.

The above conclusions are drawn based on a simplified numerical analysis. To confirm and enhance the findings of the current study, a broader set of numerical investigations should be performed in more complex cases (e.g., complex subsoil profiles, a large number of embankment heights, and several values of the surcharge loading). Furthermore, a more complex model (three-dimensional numerical simulation) would also be suggested for the design of piled embankments over soft soils. This model could be used to capture other interesting failure modes related to piled embankments, such as lateral movement and the pile bending moment at the embankment toe and could also be used to explore the slope stability of the embankment. A reliability analysis considering the uncertainties of more material properties and/or the soil spatial variability (random field method) will be developed in future studies in order to better describe the input uncertainties and obtain more precise P_f estimates.

Acknowledgments

The authors gratefully acknowledge King Mongkut's University of Technology Thonburi (KMUTT) and National Research Council of Thailand (NRCT) through grant No. NRCT5-RSA63006 and Thailand Science Research and Innovation (TSRI) under Fundamental Fund 2022 (Project: Advanced Construction Towards Thailand 4.0). The authors would also like to acknowledge the financial support provided by King Mongkut's University of Technology North Bangkok (KMUTNB) and the National Science, Research and Innovation Fund (NSRF) under Contract No. KMUTNB-FF-65-38.

References

1. Huang J, Han J, Oztoprak S. Coupled mechanical and hydraulic modelling of geosynthetic-reinforced column-supported embankments. Journal of Geotechnical and Geoenvironmental Engineering, 2009, 135(8): 1011–1021
2. Huang J, Han J. 3D coupled mechanical and hydraulic modeling of a geosynthetic-reinforced deep mixed column-supported embankment. Geotextiles and Geomembranes, 2009, 27(4): 272–280
3. Yapage N N S, Liyanapathirana D S, Kelly R B, Poulos H G, Leo C J. Numerical modeling of an embankment over soft ground improved with deep cement mixed columns: case history. Journal of Geotechnical and Geoenvironmental Engineering, 2014, 140(11): 04014062
4. Yapage N N S, Liyanapathirana D S, Poulos H G, Kelly R B, Leo C J. Numerical modeling of geotextile-reinforced embankments over deep cement mixed columns incorporating strain-softening behavior of columns. International Journal of Geomechanics, 2015, 15(2): 04014047
5. Jamsawang P, Yoobanpot N, Thanasisathit N, Voottipruex P, Jongpradist P. Three-

dimensional numerical analysis of a DCM column-supported highway embankment. Computers and Geotechnics, 2016, 72: 42–56

6. Chai J C, Shrestha S, Hino T, Ding W Q, Kamo Y, Carter J. 2D and 3D analyses of an embankment on clay improved by soil–cement columns. Computers and Geotechnics, 2015, 68: 28–37

7. Huang J, Han J. Two-dimensional parametric study of geosynthetic-reinforced column-supported embankments by coupled hydraulic and mechanical modeling. Computers and Geotechnics, 2010, 37(5): 638–648

8. Jamsawang P, Phongphinnittana E, Voottipruex P, Bergado D T, Jongpradist P. Comparative performances of two- and three-dimensional analyses of soil-cement mixing columns under an embankment load. Marine Georesources & Geotechnology, 2019, 37(7): 852–869

9. Yu Y, Bathurst R J, Damians I P. Modified unit cell approach for modelling geosynthetic-reinforced column-supported embankments. Geotextiles and Geomembranes, 2016, 44(3): 332–343

10. Lai Y P, Bergado D T, Lorenzo G A, Duangchan T. Full-scale reinforced embankment on deep jet mixing improved ground. Proceedings of the Institution of Civil Engineers - Ground Improvement, 2006, 10(4): 153–164

11. Bergado D T, Jamsawang P, Tanchaisawat T, Lai Y P, Lorenzo G A. Performance of reinforced load transfer platforms for embankments supported by deep cement mixing piles. In: GeoCongress 2008: Geosustainability and Geohazard Mitigation. Louisiana, USA, 2008, 628–637

12. Han J, Oztoprak S, Parsons R L, Huang J. Numerical analysis of foundation columns to support widening of embankments. Computers and Geotechnics, 2007, 34(6): 435–448

13. Borges J L, Marques D O. Geosynthetic-reinforced and jet grout column-supported embankments on soft soils: numerical analysis and parametric study. Computers and Geotechnics, 2011, 38(7): 883–896
14. Cheng Q, Wu J, Zhang D, Ma F. Field testing of geosynthetic-reinforced and column-supported earth platforms constructed on soft soil. Frontiers of Structural and Civil Engineering, 2014, 8(2): 124–139
15. Liu S Y, Du Y J, Yi Y L, Puppala A J. Field investigations on performance of T-shaped deep mixed soil cement column-supported embankments over soft ground. Journal of Geotechnical and Geoenvironmental Engineering, 2012, 138(6): 718–727
16. Yi Y L, Liu S Y, Puppala A J. Laboratory modelling of T-shaped soil–cement column for soft ground treatment under embankment. Géotechnique, 2016, 66(1): 85–89
17. Yi Y L, Liu S Y, Puppala A J, Jing F. Variable-diameter deep mixing column for multi-layered soft ground improvement: laboratory modeling and field application. Soils and Foundations, 2019, 59(3): 633–643
18. Yi Y L, Liu S Y, Puppala A J, Xi P S. Vertical bearing capacity behaviour of single T-shaped soil–cement column in soft ground: laboratory modelling, field test, and calculation. Acta Geotechnica, 2017, 12(5): 1077–1088
19. Yi Y L, Liu S Y, Puppala A J. Bearing capacity of composite foundation consisting of T-shaped soil-cement column and soft clay. Transportation Geotechnics, 2018, 15: 47–56
20. Yi Y L, Ni P, Liu S Y. Numerical investigation of T-shaped soil–cement column supported embankment over soft ground. In: Proceedings of China-Europe Conference on Geotechnical Engineering. Vienna, Austria, 2018, 1068–1071
21. Phutthananon C, Jongpradist P, Yensri P, Jamsawang P. Dependence of ultimate bearing capacity and failure behavior of T-shaped deep cement mixing piles on

enlarged cap shape and pile strength. Computers and Geotechnics, 2018, 97: 27–41

22. Phutthananon C, Jongpradist P, Jamsawang P. Influence of cap size and strength on settlements of TDM-piled embankments over soft ground. Marine Georesources & Geotechnology, 2020, 38(6): 686–705

23. Phutthananon C, Jongpradist P, Jongpradist P, Dias D, Baroth J. Parametric analysis and optimization of T-shaped and conventional deep cement mixing column-supported embankments. Computers and Geotechnics, 2020, 122: 103555

24. Phutthananon C, Jongpradist P, Dias D, Jamsawang P. Numerical study of the deformation performance and failure mechanisms of TDM pile-supported embankments. Transportation Geotechnics, 2021, 30: 100623

25. Phutthananon C, Jongpradist P, Jongpradist P, Dias D, Jamsawang P, Bergado D T. Performance-based design optimization of embankments resting on soft soil improved with T-shaped and conventional DCM columns. Acta Geotechnica, 2021, 16(10): 3301–3326

26. Jamsawang P, Voottipruex P, Jongpradist P, Bergado D T. Parameters affecting the lateral movements of compound deep cement mixing walls by numerical simulations and parametric analyses. Acta Geotechnica, 2015, 10(6): 797–812

27. Omine K, Ochiai H, Yasufuku N. Evaluation of scale effect on strength of cement-treated soils based on a probabilistic failure model. Soils and Foundations, 2005, 45(3): 125–134

28. Larsson S, Stille H, Olsson L. On horizontal variability in lime-cement columns in deep mixing. Géotechnique, 2005, 55(1): 33–44

29. Namikawa T, Koseki J. Effects of spatial correlation on the compression behavior of a cement-treated column. Journal of Geotechnical and Geoenvironmental Engineering, 2012, 139(8): 1346–1359

30. Liu Y, Lee F H, Quek S T, Chen E J, Yi J T. Effect of spatial variation of strength and modulus on the lateral compression response of cement-admixed clay slab. Géotechnique, 2015, 65(10): 851–865

31. Zhang R J, Hasan M S M S, Zheng J J, Cheng Y S. Effect of spatial variability of engineering properties on stability of a CSMC embankment. Marine Georesources & Geotechnology, 2018, 36(1): 91–99

32. Al-Naqshabandy M S, Bergman N, Larsson S. Strength variability in lime-cement columns based on cone penetration test data. Proceedings of the Institution of Civil Engineers - Ground Improvement, 2012, 165(1): 15–30

33. Al-Naqshabandy M S, Larsson S. Effect of uncertainties of improved soil shear strength on the reliability of embankments. Journal of Geotechnical and Geoenvironmental Engineering, 2013, 139(4): 619–632

34. Navin M P, Filz G M. Reliability of deep mixing method columns for embankment support. In: GeoCongress 2006: Geotechnical Engineering in the Information Technology Age. Georgia, USA, 2006, 1–6

35. Wijerathna M, Liyanapathirana D S. Reliability-based performance of embankments improved with deep mixing considering spatial variability of material properties. ASCE-ASME Journal of Risk and Uncertainty in Engineering Systems, Part A: Civil Engineering, 2018, 4(4): 04018035

36. Wijerathna M, Liyanapathirana D S. Significance of variability of deep cement mixed columns on the reliability of column supported embankments. International Journal of Geomechanics, 2019, 19(8): 04019087

37. Guo X, Dias D, Pan Q. Probabilistic stability analysis of an embankment dam considering soil spatial variability. Computers and Geotechnics, 2019, 113: 103093

38. Kroetz H M, Do N A, Dias D, Beck A T. Reliability of tunnel lining design using the

Hyperstatic Reaction Method. Tunnelling and Underground Space Technology, 2018, 77: 59–67

39. Guo X, Dias D. Kriging based reliability and sensitivity analysis – Application to the stability of an earth dam. Computers and Geotechnics, 2020, 120: 103411

40. Guo X, Dias D, Carvajal C, Peyras L, Breul P. A comparative study of different reliability methods for high dimensional stochastic problems related to earth dam stability analyses. Engineering Structures, 2019, 188: 591–602

41. Soubra A H, Al-Bittar T, Thajeel J, Ahmed A. Probabilistic analysis of strip footings resting on spatially varying soils using kriging metamodeling and importance sampling. Computers and Geotechnics, 2019, 114: 103107

42. Pan Q, Dias D. Sliced inverse regression-based sparse polynomial chaos expansions for reliability analysis in high dimensions. Reliability Engineering and System Safety, 2017, 167: 484–493

43. Echard B, Gayton N, Lemaire M. AK-MCS: An active learning reliability method combining Kriging and Monte Carlo Simulation. Structural Safety, 2011, 33(2): 145–154

44. Al-Bittar T, Soubra A H, Thajeel J. Kriging-based reliability analysis of strip footings resting on spatially varying soils. Journal of Geotechnical and Geoenvironmental Engineering, 2018, 144(10): 04018071

45. El Haj A K, Soubra A H, Fajoui J. Probabilistic model of an offshore monopile foundation taking into account the soil spatial variability. Computers and Geotechnics, 2019, 106: 205–216

46. Zhou S, Guo X, Zhang Q, Dias D, Pan Q. Influence of a weak layer on the tunnel face stability – Reliability and sensitivity analysis. Computers and Geotechnics, 2020, 122: 103507

47. Jongpradist P, Jamsawang P, Kongkitkul W. Equivalent void ratio controlling the mechanical properties of cementitious material-clay mixtures with high water content. Marine Georesources & Geotechnology, 2019, 37(10): 1151–1162

48. Jongpradist P, Homtragoon W, Sukkarak R, Kongkitkul W, Jamsawang P. Efficiency of rice husk ash as cementitious material in high-strength cement-admixed clay. Advances in Civil Engineering, 2018, 2018: 8346319

49. Huang J, Kelly R, Sloan S W. Stochastic assessment for the behaviour of systems of dry soil mix columns. Computers and Geotechnics, 2015, 66: 75–84

50. Schöbi R, Sudret B, Marelli S. Rare event estimation using Polynomial-Chaos Kriging. ASCE-ASME Journal of Risk and Uncertainty in Engineering Systems, Part A: Civil Engineering, 2017, 3(2): D4016002

51. Marelli S, Sudret B. UQLab: a framework for uncertainty quantification in Matlab. In: Proceedings of the 2nd International Conference on Vulnerability, Risk Analysis and Management (ICVRAM2014). Liverpool, United Kingdom, 2014, 2554–2563

52. Kasama K, Whittle A J, Zen K. Effect of spatial variability on the bearing capacity of cement-treated ground. Soils and Foundations, 2012, 52(4): 600–619

53. Bhasi A, Rajagopal K. Geosynthetic-reinforced piled embankments: comparison of numerical and analytical methods. International Journal of Geomechanics, 2014, 15(5): 04014074

54. Brinkgreve R B J, Kumarswamy S, Swolfs W M, Zampich L, Ragi Manoj N. PLAXIS 2D Material model manual. Plaxis bv., The Netherlands, 2019

55. Schanz T, Vermeer A, Bonnier P. The hardening soil model: formulation and verification. In: Proceedings of 1st international PLAXIS symposium on beyond 2000 in computational geotechnics. Amsterdam, the Netherlands, 1999, 281–296

56. Jamsawang P, Voottipruex P, Tanseng P, Jongpradist P. Effectiveness of deep cement

mixing walls with top-down construction for deep excavations in soft clay: case study and 3D simulation. Acta Geotechnica, 2019, 14(1): 225–246

57. Waichita S, Jongpradist P, Jamsawang P. Characterization of deep cement mixing wall behavior using wall-to-excavation shape factor. Tunnelling and Underground Space Technology, 2019, 83: 243–253

58. Wonglert A, Jongpradist P, Jamsawang P, Larsson S. Bearing capacity and failure behaviors of floating stiffened deep cement mixing columns under axial load. Soils and Foundations, 2018, 58(2): 446–461

59. Surarak C, Likitlersuang S, Wanatowski D, Balasubramaniam A, Oh E, Guan H. Stiffness and strength parameters for hardening soil model of soft and stiff Bangkok clays. Soils and Foundations, 2012, 52(4): 682–697

60. Jamsawang P, Voottipruex P, Boathong P, Mairaing W, Horpibulsuk S. Three-dimensional numerical investigation on lateral movement and factor of safety of slopes stabilized with deep cement mixing column rows. Engineering Geology, 2015, 188: 159–167

61. Goh A T C, Zhang F, Zhang W, Zhang Y, Liu H. A simple estimation model for 3D braced excavation wall deflection. Computers and Geotechnics, 2017, 83: 106–113

62. Hsiung B C B, Yang K H, Aila W, Ge L. Evaluation of the wall deflections of a deep excavation in Central Jakarta using three-dimensional modeling. Tunnelling and Underground Space Technology, 2018, 72: 84–96

63. Waichita S, Jongpradist P, Schweiger H F. Numerical and experimental investigation of failure of a DCM-wall considering softening behaviour. Computers and Geotechnics, 2020, 119: 103380

64. Okyay U S, Dias D. Use of lime and cement treated soils as pile supported load transfer platform. Engineering Geology, 2010, 114(1–2): 34–44

65. Ma H, Luo Q, Wang T, Jiang H, Lu Q. Numerical stability analysis of piled embankments reinforced with ground beams. Transportation Geotechnics, 2020, 26: 100427

66. Zhuang Y, Wang K. Finite element analysis on the dynamic behavior of soil arching effect in piled embankment. Transportation Geotechnics, 2018, 14: 8–21

67. Hamrouni A, Dias D, Sbartai B. Soil spatial variability impact on the behavior of a reinforced earth wall. Frontiers of Structural and Civil Engineering, 2020, 14(2): 518–531

68. Das B M. Fundamentals of geotechnical engineering. Cengage Learning, 2007

69. Kulhawy F H, Mayne P W. Manual on estimating soil properties for foundation design. Rep. No. EPRI-EL-6800. Ithaca, New York: Cornell University, 1990

70. Phoon K K, Kulhawy F H. Characterization of geotechnical variability. Canadian Geotechnical Journal, 1999, 36(4): 612–624

Table 1 Summary of random variable parameters used in the reliability analysis

Variable	Unit	Distribution	μ	σ	COV		References
					Mean	Range	
$s_{u,\,\mathrm{soil}}$	kPa	Log-normal	15	3.6	24%	4-44%	Phoon and Kulhawy [70]
$q_{u,\,\mathrm{pile}}$	kPa	Log-normal	200	100	50%	30-70%	< 60% Larsson et al. [28] 20-40% Namikawa and Koseki [29] 25-55% Liu et al. [30] 22-67% Al-Naqshabandy et al. [32] 30-70% Wijerathna and Liyanapathirana [35,36]
γ_{emb}	kN/m^3	Log-normal	16	1.44	9%	3-20%	Phoon and Kulhawy [70]

Note: μ = mean; σ = standard deviation; COV = coefficient of variation; $s_{u,\,\mathrm{soil}}$ = undrained shear strength of soil; $q_{u,\,\mathrm{pile}}$ = unconfined compressive strength of pile; γ_{emb} = unit weight of embankment.

Table 2 Simulation process of the numerical modeling

Stage	Details	Duration (days)
1	Generation of the initial stresses using the coefficient of lateral earth pressure at rest and soil unit weight	-
2	Installation of the soil-cement pile (disregard the pile installation effect)	-
3	Construction of a 1.5-m-high embankment fill and initialize the displacements at the end of this stage	-
4	Installation of a 0.2-m-thick concrete slab	-
5	Apply a surcharge load of 25 kPa on the top of the concrete slab	-
6	Consolidation after end of stage construction (> 90% degree of consolidation)	1500

Table 3 Material properties in the Hardening Soil (HS) model used for soft soils [22]

Parameters	Symbols	Soft clay
Unit weight (kN/m^3)	γ	15
Secant stiffness (kPa)	E_{50}^{ref}	2,400 ($E_{50}^{ref} = 160 s_{u,\,\mathrm{soil}}$)
Tangential stiffness (kPa)	E_{oed}^{ref}	2,400 ($E_{oed}^{ref} = E_{50}^{ref}$)
Unloading and reloading stiffness (kPa)	E_{ur}^{ref}	7,200 ($E_{ur}^{ref} = 3E_{50}^{ref}$)
Poisson's ratio for unloading-reloading (-)	ν_{ur}	0.20
Power of the stress level dependency of the stiffness (-)	m	1
Effective cohesion (kPa)	c'	2
Effective friction angle (degree)	ϕ'	22
Over consolidation ratio (-)	OCR	1.1
Permeability-vertical direction (m/day)	k_y	0.1×10^{-3}
Permeability-horizontal direction (m/day)	k_x	0.2×10^{-3}

Note: $s_{u,\,\mathrm{soil}}$ = undrained shear strength; reference stress for stiffnesses (p^{ref}) = 100 kPa; at-rest earth pressure coefficient for over-consolidated clay (K_0^{OC}) = $(1-\sin\phi')\times \mathrm{OCR}^{\sin\phi'}$.

Table 4 Material properties in the Mohr–Coulomb (MC) model used for the soil–cement mixing (SCM) piles and embankment fill and in the linear elastic (LE) model used for the concrete slab

Parameters	Symbols	SCM pile	Embankment fill[a]	Concrete slab
Material model	-	MC	MC	LE
Unit weight (kN/m^3)	γ	15	16	25
Elastic modulus (kPa)	E'	$100q_{u,\,\mathrm{pile}}$	3,000	1×10^7
Poisson's ratio (-)	ν'	0.33	0.25	0.20
Effective cohesion (kPa)	c'	$c_u = 0.5q_{u,\,\mathrm{pile}}$	10	-
Effective friction angle (degree)	ϕ'	25	26	-
Permeability-vertical direction (m/day)	k_y	0.1×10^{-3}	-	-
Permeability-horizontal direction (m/day)	k_x	0.2×10^{-3}	-	-

Note: $q_{u,\,\mathrm{pile}}$ = pile unconfined compressive strength; $q_{u,\,\mathrm{pile}}$ of reference case is 200 kPa. [a]Data of embankment fill from Phutthananon et al. [22].

Table 5 Case investigated in the parametric study

Parameters	Unit	DCM	TDM#1	TDM#2	TDM#3	TDM#4	TDM#5
D_{TDM} or D_{DCM}	m	0.80	1.00	1.15	1.31	1.40	1.50
d_{TDM}	m	-	0.50	0.50	0.50	0.50	0.50
H	m	-	3.12	2.18	1.60	1.37	1.17
L_{TDM} or L_{DCM}	m	6.00	6.00	6.00	6.00	6.00	6.00
V_p	m^3	3.02	3.02	3.02	3.02	3.02	3.02
α_s	-	1.0	1.6	2.2	3.0	3.5	4.0
a_r	%	12.57	19.63	25.97	33.70	38.48	44.18

Note: D_{TDM} = TDM pile head diameter; D_{DCM} = DCM pile head diameter; d_{TDM} = TDM pile body diameter; H = thickness of TDM pile cap; L_{TDM} = TDM pile length; L_{DCM} = DCM pile length; V_p = pile volume; α_s = pile shape factor; a_r = area improvement ratio at shallow depth.

Table 6 Parameters used in the parametric study to investigate the effects of the variabilities of soil parameters

Parameters	Unit	Range of values
μ-$s_{u,\,\mathrm{soil}}$	kPa	5, 10, 15, 20, 25
COV-$s_{u,\,\mathrm{soil}}$	-	0.04, 0.24, 0.44
μ-$q_{u,\,\mathrm{pile}}$	kPa	200, 300, 400, 500, 600, 700, 800
COV-$q_{u,\,\mathrm{pile}}$	-	0.3, 0.5, 0.7
μ-γ_{emb}	kN/m^3	14, 15, 16, 18, 20
COV-γ_{emb}	-	0.03, 0.09, 0.20

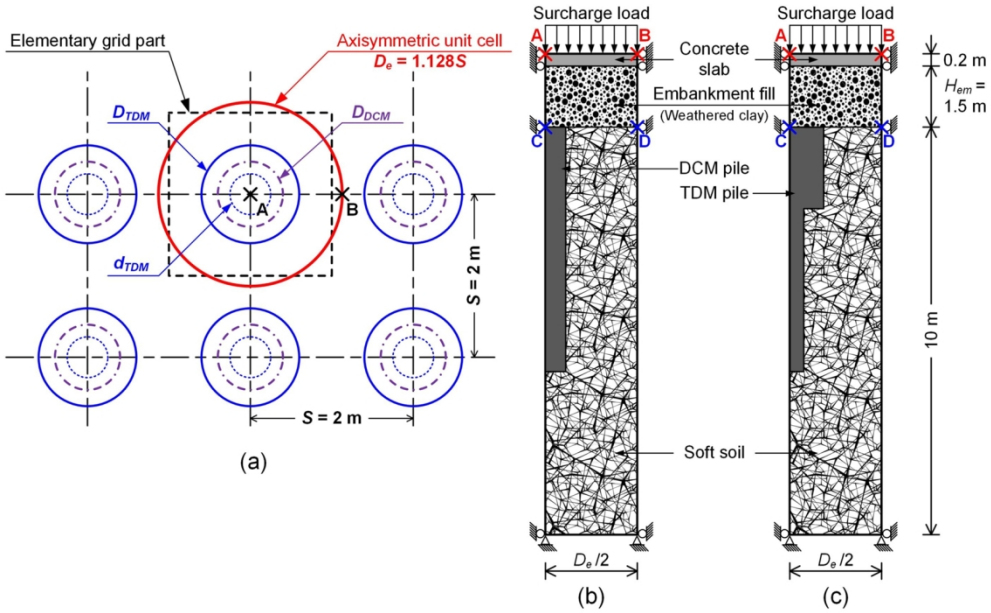

Fig. 1

150x93mm (300 x 300 DPI)

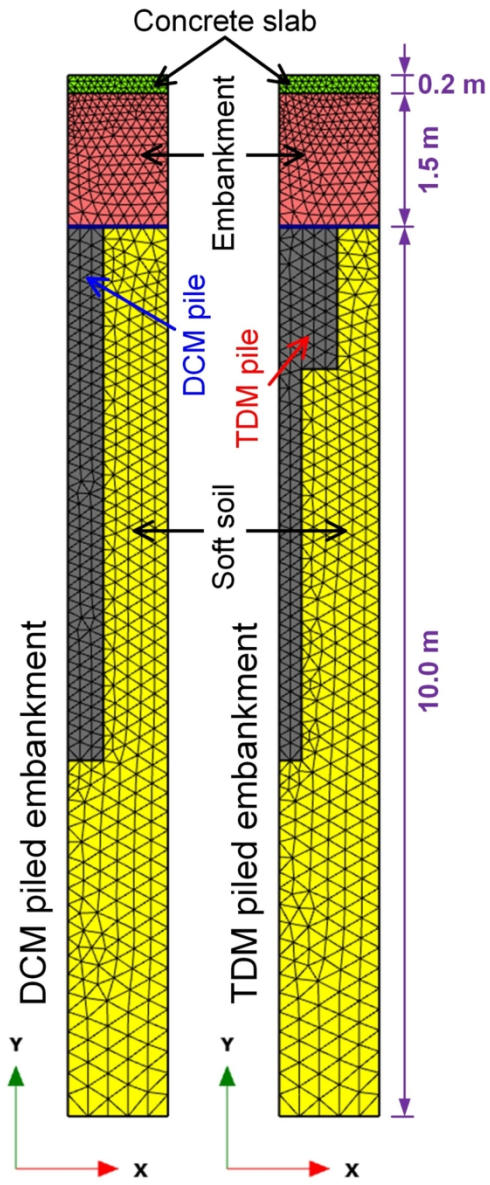

Fig. 2

74x179mm (300 x 300 DPI)

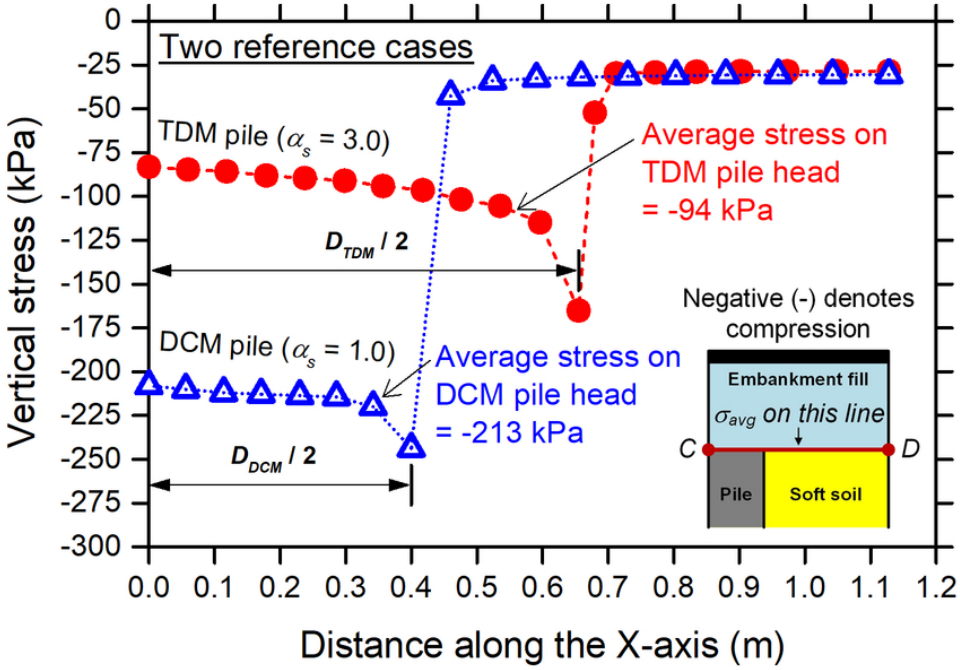

Fig. 3

74x51mm (300 x 300 DPI)

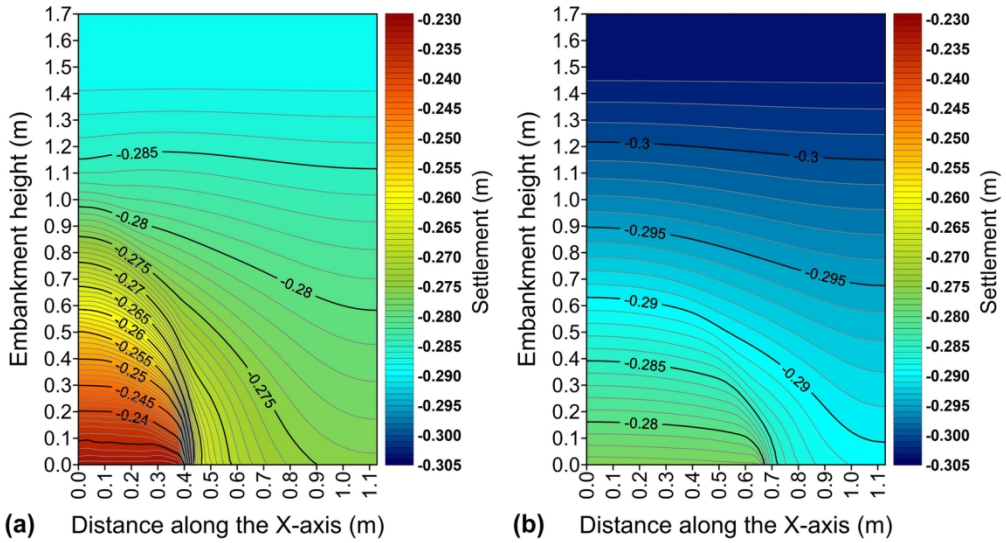

Fig. 4

149x80mm (300 x 300 DPI)

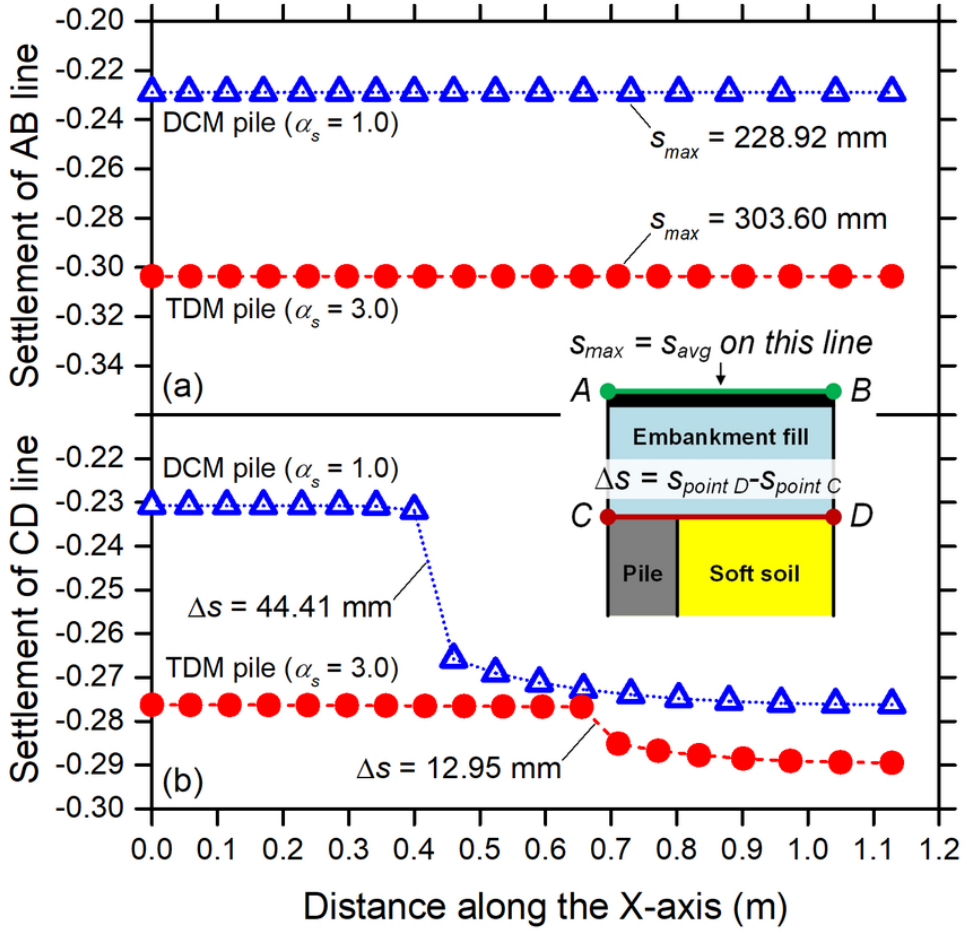

Fig. 5

74x70mm (300 x 300 DPI)

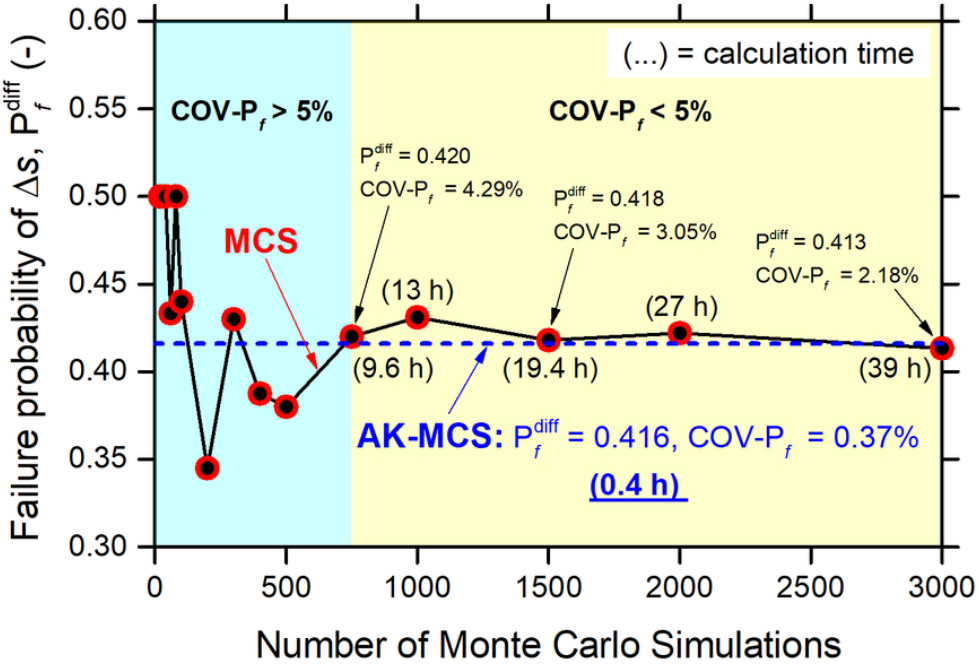

Fig. 6

74x51mm (300 x 300 DPI)

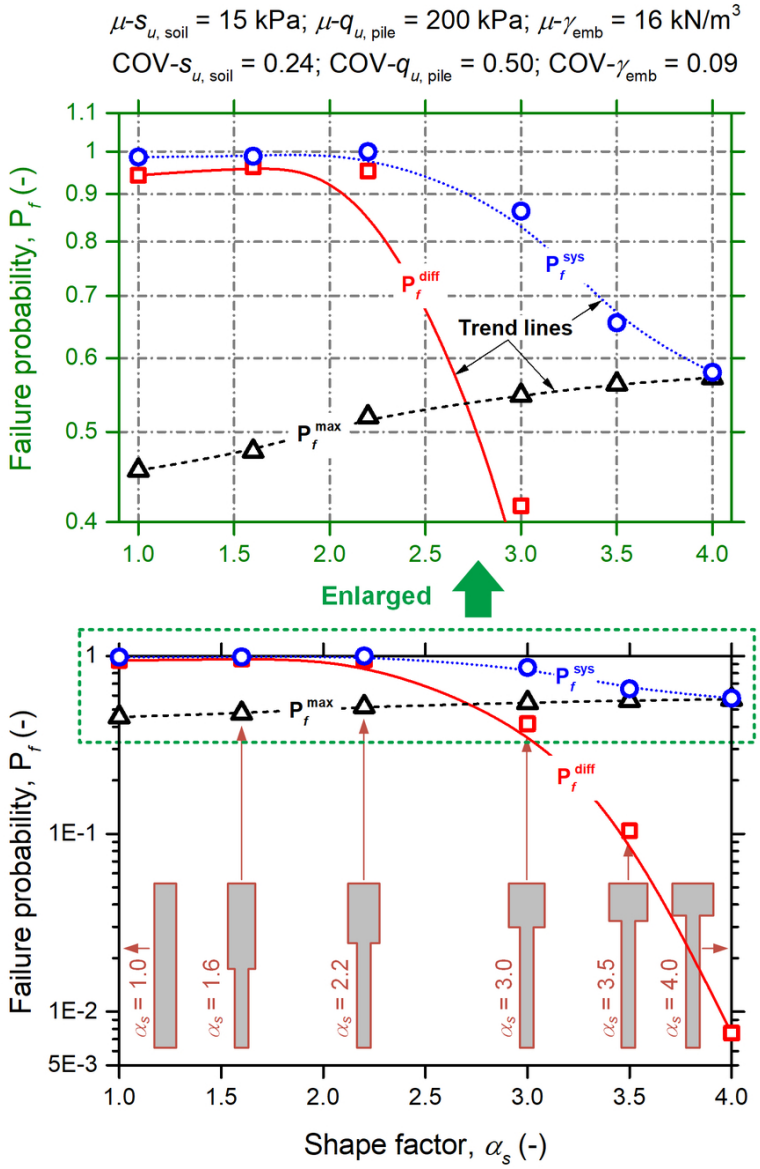

Fig. 7

74x115mm (300 x 300 DPI)

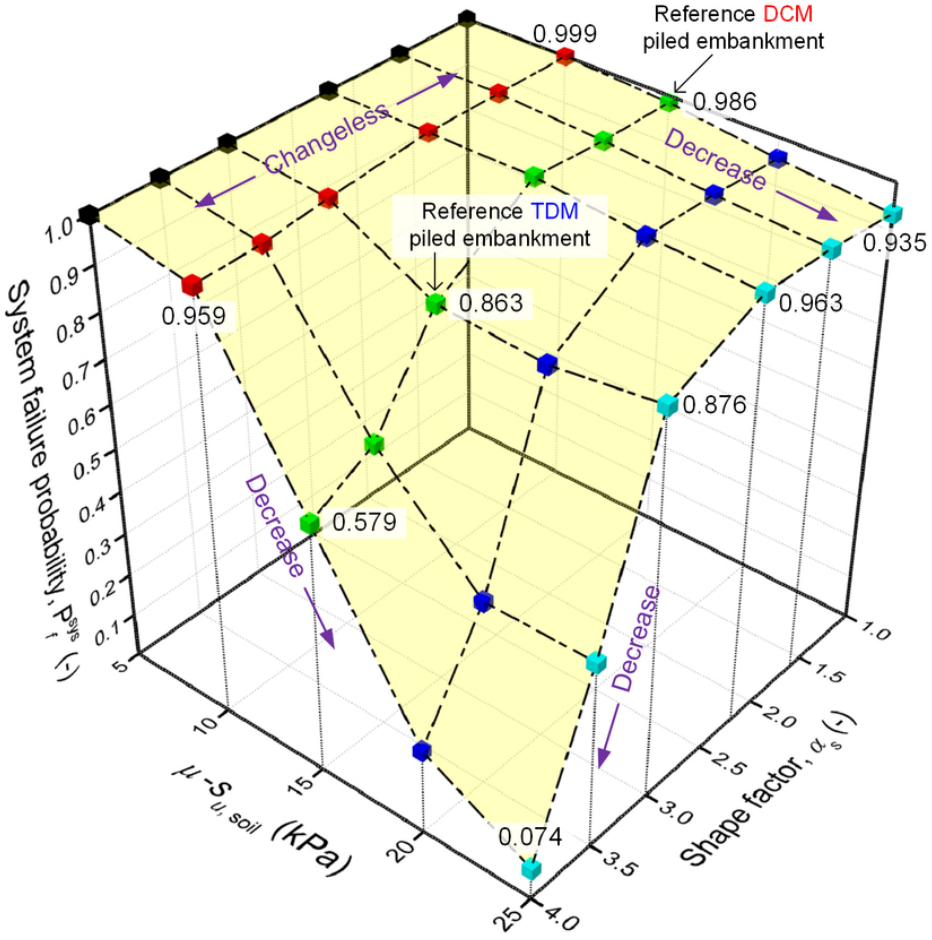

Fig. 8

74x74mm (300 x 300 DPI)

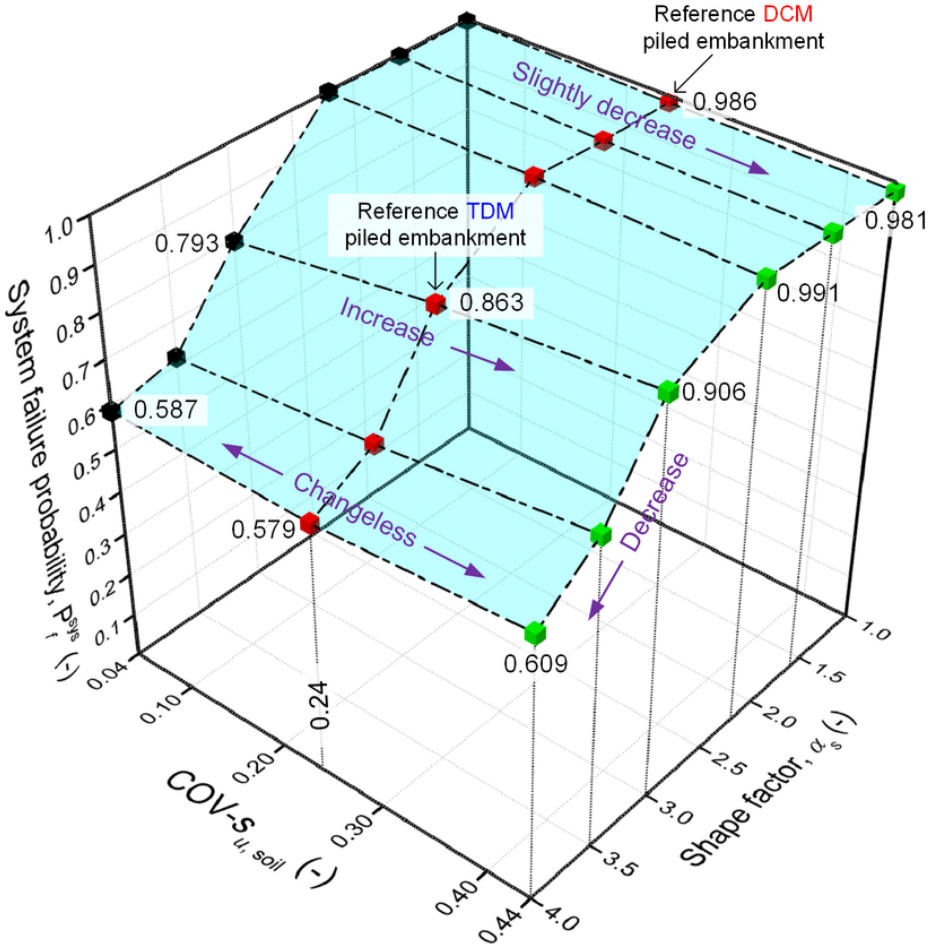

Fig. 9

74x74mm (300 x 300 DPI)

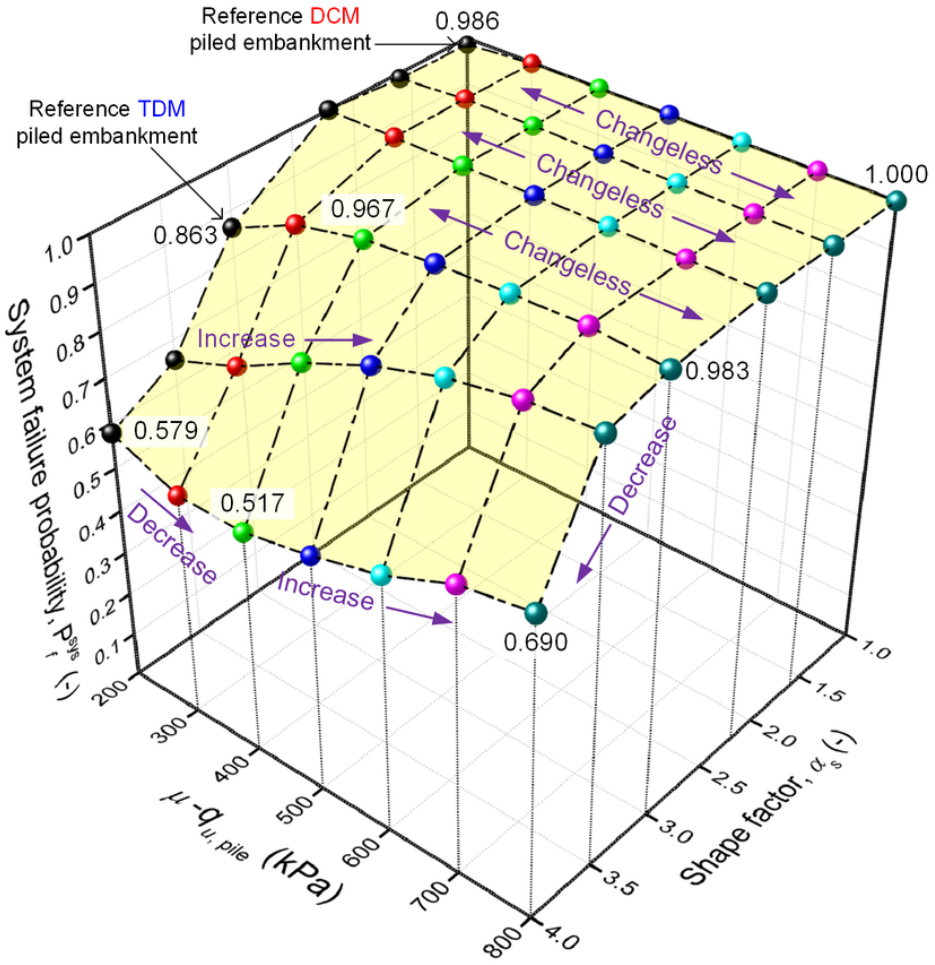

Fig. 10

74x74mm (300 x 300 DPI)

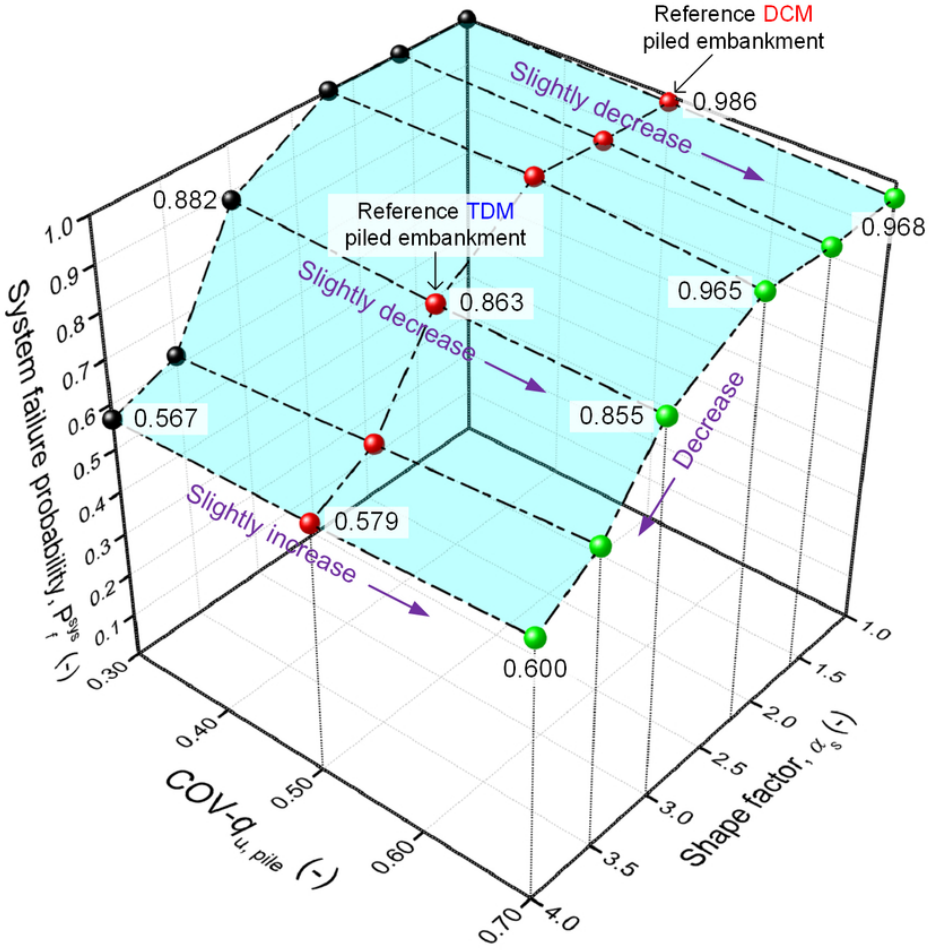

Fig. 11

74x74mm (300 x 300 DPI)

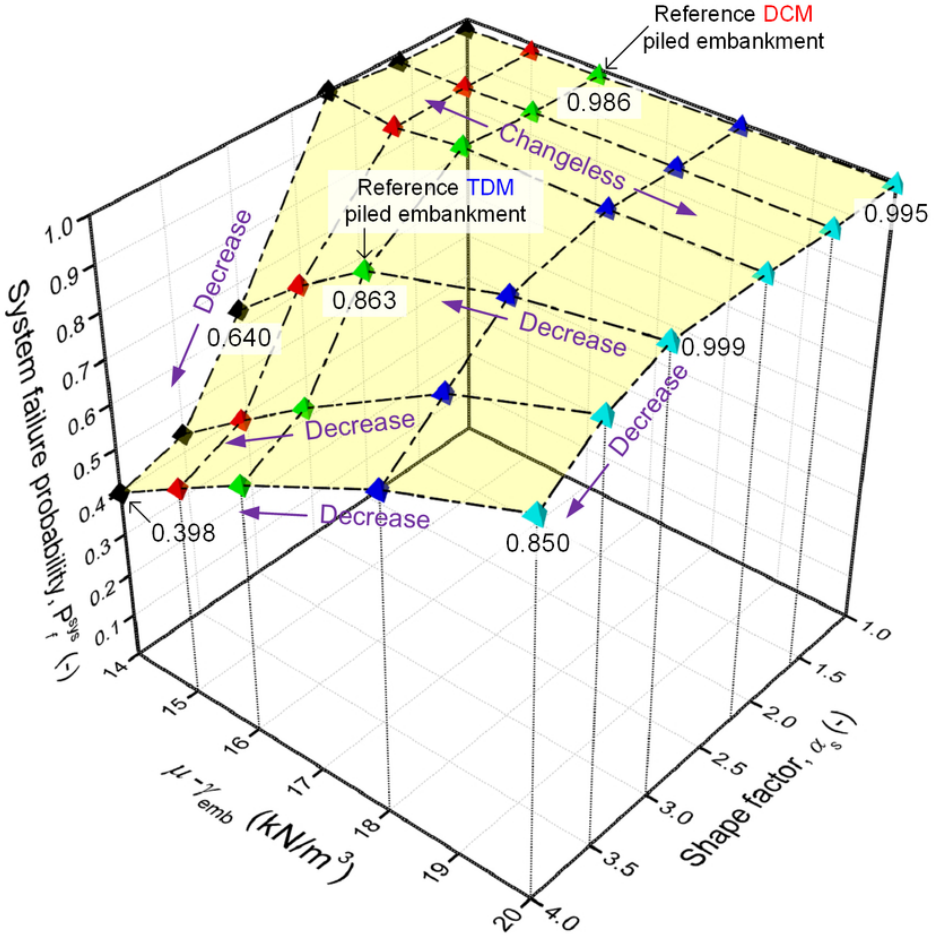

Fig. 12

74x74mm (300 x 300 DPI)

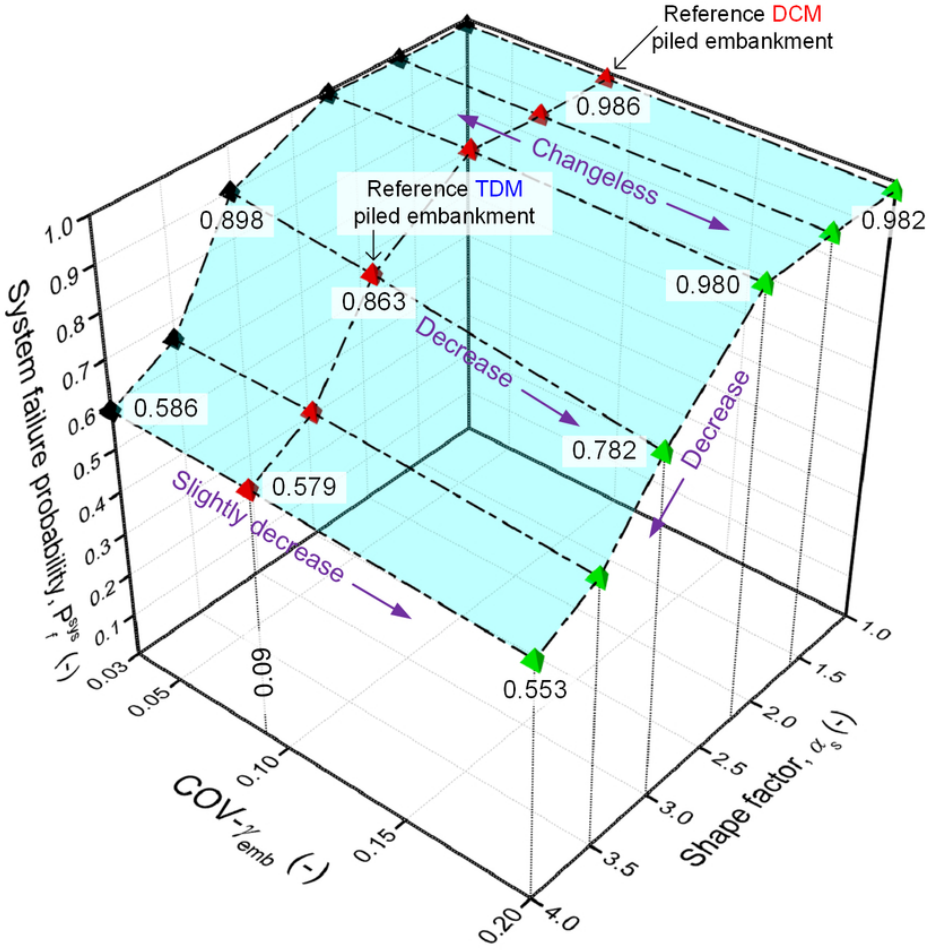

Fig. 13

74x74mm (300 x 300 DPI)